(p,d) reaction at 800 MeV

G. R. Smith,* J. R. Shepard, R. L. Boudrie,† and R. J. Peterson
Nuclear Physics Laboratory, University of Colorado, Boulder, Colorado 80309

G. S. Adams,‡ T. S. Bauer,* G. J. Igo, G. Pauletta, C. A. Whitten, Jr., and A. Wriekat§
University of California at Los Angeles, Los Angeles, California 90024

B. Hoistad**
Los Alamos Meson Physics Facility, Los Alamos, New Mexico 87545

G. W. Hoffmann
University of Texas, Austin, Texas 78712 and Los Alamos Meson Physics Facility, Los Alamos, New Mexico 87545
(Received 2 March 1984)

The neutron pickup reaction (p,d) has been studied at a proton energy of 800 MeV on targets of ^{7}Li, ^{12}C, ^{13}C, ^{16}O, ^{25}Mg, ^{28}Si, and ^{40}Ca. States known to correspond to single-hole excitations are seen and in most cases the data are properly understood through distorted-wave Born approximation calculations. High-spin final states are prominent, and some are shown to be excited through multiple step processes. The strongest states seen in the data do not correspond to known levels.

I. INTRODUCTION

The "pickup" picture of the (p,d) reaction is an appealing one because of its simplicity. The process is envisioned as one in which a single neutron is removed from the target nucleus in one step. It is obvious that such a reaction could give information about the single particle wave functions of the nuclear shell model. For many years this simple picture has been profitably used at low bombarding energies to extract useful information about the quantum numbers and parentage of single hole states of nuclei. Also, due to its simplicity, the (p,d) process and its time-reversed twin, (d,p), have frequently been the focus of attention for reaction theorists who use it as a test bed for theoretical treatment of nuclear rearrangement scattering. The usual theoretical treatment for the low energy (p,d) reaction is the distorted wave Born approximation (DWBA) which directly incorporates the single-step picture. The DWBA has been quite successful in describing (p,d) transitions to single hole levels.

With the development of intermediate energy facilities it has become possible to measure (p,d) cross sections to discrete nuclear levels at $T_p \geq 200$ MeV. The most obvious new feature at high beam energies is the large asymptotic momentum transfer, $|\vec{k}_p - \vec{k}_d| = 1.7$ and 2.5 fm^{-1} for the $T = 800$ MeV ^{13}C(p,d)^{12}C(g.s.) reaction at $\theta_{c.m.} = 0°$ and 25°, respectively, as compared with values of 0.3 and 0.6 fm^{-1} for $T_p = 30$ MeV. These larger momenta are appreciably above the Fermi momenta (~ 1.4 fm^{-1}) of valence nucleons. Hence, if the momentum occurs primarily on a single nucleon—as in the low energy picture of the reaction—the process should reflect new details of the momentum space wave function of that nucleon. On the other hand, these momenta are appreciably above the characteristic pion momentum given by $k_\pi = m_\pi c/\hbar = 0.7$ fm^{-1}. The proton bombarding energies are also well above the pion production threshold. In fact, the π-production cross section for NN scattering is known to exceed the (non-Coulomb) elastic cross section at these energies. Consequently, specific intermediate pion states might play such an important role that the low energy model is fundamentally inappropriate and the (p,d) reaction cannot reflect the nature of single particle wave functions in any direct way. A quantitative understanding of the reaction mechanism must be achieved before new and interesting nuclear structure information could be extracted from intermediate energy (p,d) measurements, where the spectra do show strong population of different states from those prominent at lower energies. Therefore those measurements should be made which are most likely to aid in unraveling reaction mechanism effects. This suggests the use of target nuclei which have been extensively studied at lower energies where the nuclear structure of the initial and final levels is reasonably well established.

Previous experimental studies[1–9] of the intermediate energy (p,d) reaction on target nuclei with $A \geq 4$ have indeed concentrated on such nuclei. However, these experiments have been limited to the measurement of a few strong transitions for a single light target (^{4}He, ^{12}C, or ^{13}C). Published theoretical interpretations of these data[1–3,6,8–13] have also been quite restricted, usually focusing on a single transition and generally using a simple theoretical approach warranting a qualitative comparison at most.

In the present study we present data for the $T_p = 800$ MeV (p,d) reaction covering many transitions in each of several target nuclei having $7 \leq A \leq 40$. With such a relatively large body of data important systematic features of the reaction can more readily be established. The specific analysis presented here will focus exclusively on a careful extension of the low energy DWBA technique, a model which has been well validated and extensively used in the

lower energy realm. If it can be shown to describe intermediate energy data adequately we can move beyond questions of reaction mechanism and use the (p,d) reaction as a nuclear probe. If the DWBA approach fails, the manner of the failure is likely to give valuable clues as to the true nature of the reaction mechanism.

II. EXPERIMENTAL METHOD

The 800 MeV (p,d) reaction was measured on targets of ^{7}Li, ^{12}C, ^{13}C, ^{16}O, ^{25}Mg, ^{28}Si, and ^{40}Ca at the Los Alamos Meson Physics Facility (LAMPF). The deuterons were detected in the high resolution spectrometer (HRS).[14] Excellent particle identification was obtained by utilizing a 1.5 m time-of-flight path between two scintillators at the spectrometer focal plane. These scintillators also provided differential energy loss information which was used in conjunction with the time-of-flight information.

Three independent methods of incident proton beam monitoring were employed in the (p,d) measurements. The most reliable of these methods employed two sets of monitor telescopes situated at $\pm 120°$ with respect to the incident beam. Each telescope consisted of four small plastic scintillators in coincidence and subtended a solid angle of 0.28 msr.

The monitor telescopes were normalized to the various targets in an absolute fashion by comparison to a secondary emission monitor located downstream from the scattering chamber. Additionally, ion chambers situated in the scattering chamber permitted a useful check of the above methods at various angles. Since the monitor telescopes were the only devices which were operable over the entire range of incident beam current (1—100 nA) and scattering angle (3°—40°), they were chosen to provide the relative normalization of the data.

The relative acceptance as a function of the focal plane position was carefully checked by sweeping strongly populated peaks across the focal plane in momentum steps of approximately $\frac{1}{2}\%$. The peaks used were the ground state and 6.48 MeV $\frac{7}{2}^-$ state of ^{11}C resulting from the 800 MeV ^{12}C(p,d)^{11}C reaction. The acceptance was found to be uniform in the region of interest, to within the experimental errors.

Considerable improvement in the energy resolution of the final excitation energy spectra then resulted by making software corrections to observed correlations in the data between excitation energy and both particle momentum and the reaction angles. The various correlations were removed by including a polynomial series in the directly measured quantities from the wire chambers at the focal plane. The coefficients of the polynomial series for each correlation were determined from a least squares fit to rays representing the experimentally measured wire chamber quantities.

The absolute normalization of the data was performed using three independent methods. First, data were taken for p + H elastic scattering as well as ^{12}C(p,d)^{11}C on the same $C_{10}H_{11}$ target. The ^{12}C(p,d)^{11}C cross section was then expressed in terms of the known p-H elastic scattering cross section. A second measurement was performed to ensure that the solid angle for p + H elastic scattering was the same as that or the much higher spectrometer fields demanded by the (p,d) reaction. This was accomplished by inserting a small (0.26 msr) solid angle defining aperture at the spectrometer entrance. This method agreed with the measurements without the aperture to within 3%. Finally, the ^{2}H(p,d)^{1}H and ^{12}C(p,d)^{11}C reactions were measured on the same CD_2 target. These measurements were then compared to known back angle neutron-deuteron elastic scattering data.[15] This technique independently confirmed the other absolute normalizations; agreement was better than 3%.

Due to the low ($\lesssim 10$ μb/sr) differential cross sections for the (p,d) reaction at this energy, relatively thick targets were used. The ^{12}C targets consisted of a Pilot B scintillator ($C_{10}H_{11}$) containing natural carbon (99% ^{12}C) and had total areal densities of 173 and 328 mg/cm^2. The 99% isotopically pure ^{25}Mg target had a thickness of 101 mg/cm^2. The natural silicon targets (92% ^{28}Si) had thicknesses of 86, 306, and 475 mg/cm^2. The areal densities and purities of the various ^{40}Ca targets were 48.4 (100% ^{40}Ca), 235 (97% ^{40}Ca), and 470 mg/cm^2 (97% ^{40}Ca). The error in the target thicknesses was taken to be $\pm 3\%$.

The ^{16}O target thickness was 458 mg/cm^2 $\pm 8\%$. Since a water target was used, special attention was devoted to this target thickness measurement. The ^{16}O target consisted of distilled water introduced between two thin Mylar sheets. These sheets bowed out in the vacuum of the scattering chamber, so the nonuniform ^{16}O target thickness was obtained by measuring the known p + H elastic scattering reaction on the hydrogen present in the H_2O target at two scattering angles. Uncertainties arising from this nonuniform density, or leaks or bubbles in the target, were accounted for by simply using the monitor telescopes for all subsequent normalizations.

Including uncertainties associated with the normalization cross sections, target thickness, monitors, and solid angles, the final error in absolute normalization for these data is $\pm 8\%$, except for ^{16}O where the error is $\pm 12\%$ due to the greater uncertainty in the target thickness.

III. EXPERIMENTAL RESULTS

A. Introduction

Using the experimental techniques described in Sec. II, (p,d) reaction spectra were measured for targets of ^{7}Li, ^{12}C, ^{13}C, ^{16}O, ^{25}Mg, ^{28}Si, and ^{40}Ca. Roughly 25 MeV of excitation energy was covered in each spectrum. Measurements on light targets ($A < 13$) spanned an angular range of roughly 3° to 40° in the laboratory frame. For the heavier targets a range of $3° \lesssim \theta_{lab} \lesssim 25°$ was covered. These angles correspond to asymptotic momentum transfers ($\vec{q} = \vec{k}_p - \vec{k}_d$) of roughly $2 < q < 6$ fm^{-1} in the center-of-mass system. In general, an energy resolution of roughly 400 keV (FWHM) was achieved. Energy calibration of the spectra was accomplished by assuming the high resolution spectrometer (HRS) focal plane position response was linear in excitation and the calibration was based on known levels excited in the ^{12}C, ^{13}C, and ^{25}Mg (p,d) reactions. Each spectrum for each target was cali-

brated by identifying the ground state of the residual nucleus and at least one known strongly populated excited state. In the cases of ^{28}Si and ^{40}Ca where no strong known excited state could be located, the dispersion (MeV/channel) was determined from either a ^{12}C or ^{25}Mg (p,d) spectrum accumulated at the same time as the spectrum to be calibrated. Peak areas were determined by a least square fitting procedure using the code SPECTR.[16]

Although the data for the ^{7}Li and ^{13}C (p,d) reactions have appeared in an earlier, preliminary paper,[9] we also include them here in order to provide a more comprehensive picture of the (p,d) reaction at $T_p = 800$ MeV and to include more complete theoretical discussions.

B. ^{7}Li(p,d)^{6}Li

A typical spectrum measured for the ^{7}Li(p,d)^{6}Li reaction at $T_p = 800$ MeV appears in Fig. 1 and a list of the observed levels appears in Table I. The spectrum is dominated by two levels, the 1^+ $T=0$ ground state and the

TABLE I. Known levels excited in the (p,d) reaction at $T_p = 800$ MeV. Note the following: bracketed states are not resolved.

Target	Level		Target	Level[a]	
	E_x (MeV)	J^π, T		E_x (MeV)	J^π, T
^{7}Li	0.0	$1^+,0$	^{25}Mg	0.0	$0^+,0$
	2.18	$3^+,0$		1.37	$2^+,0$
	5.37	$2^+,1$		4.12	$4^+,0$
	5.65	$1^+,0$		12.39±0.18	
^{12}C	0.0	$\frac{3}{2}^-,\frac{1}{2}$		13.30±0.18	
	2.00	$\frac{1}{2}^-,\frac{1}{2}$		14.13±0.20	
	4.32	$\frac{5}{2}^-,\frac{1}{2}$		15.17±0.20	
	4.80	$\frac{3}{2}^-,\frac{1}{2}$		15.68±0.20	
	6.48	$\frac{7}{2}^-,\frac{1}{2}$		16.56±0.20	
	8.10	$\frac{3}{2}^-,\frac{1}{2}$		0	$\frac{5}{2}^+,\frac{1}{2}$
	8.42	$\frac{5}{2}^-,\frac{1}{2}$	^{28}Si	0.78	$\frac{1}{2}^+,\frac{1}{2}$
	8.66	$\frac{7}{2}^+,\frac{1}{2}$		0.96	$\frac{3}{2}^+,\frac{1}{2}$
	8.70	$\frac{5}{2}^+,\frac{1}{2}$		2.65	$\frac{5}{2}^+,\frac{1}{2}$
	9.98±0.2			2.87	$(\frac{3}{2},\frac{5}{2})^+,\frac{1}{2}$
	10.56±0.2			2.91	$\frac{9}{2}^+,\frac{1}{2}$
	13.22±0.25[a]			4.20±0.15	
^{13}C	0.0	$0^+,0$		4.57±0.20	
	4.44	$2^+,0$		5.37±0.15	
	9.64	$3^-,0$ (weak)		6.57±0.30	
	12.71	$1^+,0$		7.18±0.15	
	14.08	$4^+,0$		8.32±0.15	
	15.11	$1^+,1$		9.59±0.18	
	16.11	$2^+,1$		11.65±0.20	
	20.61±0.04			14.79±0.25	
	25.4±0.1[a]			15.28±0.25	
^{16}O	0.0	$\frac{1}{2}^-,\frac{1}{2}$		15.74±0.25	
	5.18	$\frac{1}{2}^+,\frac{1}{2}$		16.25±0.25	
	5.24	$\frac{5}{2}^+,\frac{1}{2}$	^{40}Ca	0.00	
	6.18	$\frac{3}{2}^-,\frac{1}{2}$		2.68±0.20	
	7.28	$\frac{7}{2}^+,\frac{1}{2}$		3.79±0.20	
	7.56	$\frac{1}{2}^+,\frac{1}{2}$		5.40±0.20	
	8.84±0.15			6.39±0.25	
	10.42±0.15			7.26±0.25	
	10.87±0.15			7.78±0.25	
	12.21±0.15			10.92±0.30[a]	
	13.59±0.15			17.8 ±0.50[a]	
	19.02±0.20[a]				
	21.11±0.20[a]				

[a]Width ≥ 500 keV.

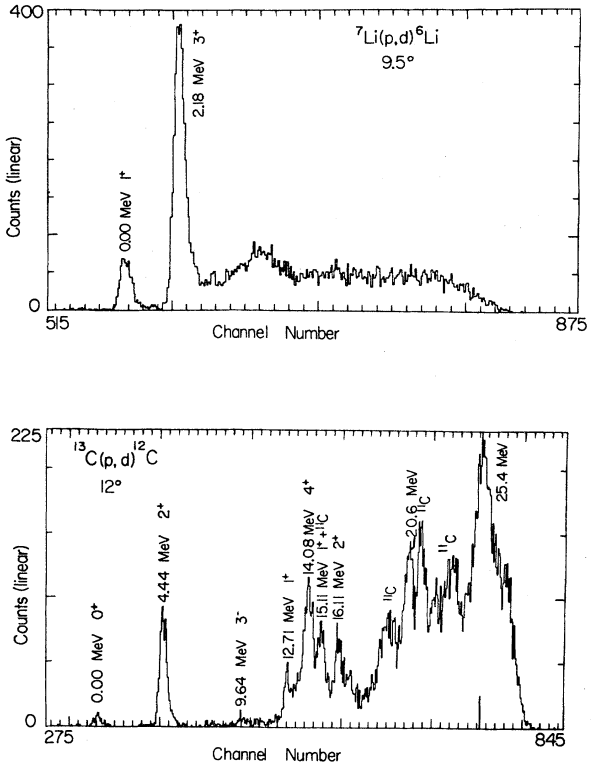

FIG. 1. Deuteron spectra from 800 MeV protons incident upon targets of ^{7}Li and ^{13}C are shown. The scales are linear in excitation energy.

2.18 MeV 3^+ $T=0$ level. No appreciable excitation of the 3.56 MeV 0^+ $T=1$ level is observed. A broad, relatively weak structure at 5.5 MeV is seen which probably contains contributions from the 5.37 MeV 2^+ $T=1$ and 5.65 MeV 1^+ $T=0$ unbound levels.

This spectrum is quite different from that observed at lower energies.[17–22] The most striking difference is the strong enhancement of the 2.18 MeV 3^+ level relative to the 1^+ ground state at $T_p=800$ MeV. At this energy the ratio of the 3^+ to the 1^+ cross section is about 6 to 1. The low energy measurements, with $30.3 \leq T_p \leq 185$ MeV, all give a ratio of roughly unity. The low energy ratio is roughly consistent with the ratio of spectroscopic factors calculated using reasonable models for the structure of ^{6,7}Li.[19] The origin of the 3^+ enhancement is not known, although it is probably a consequence of the large momentum mismatch ($q = |\vec{k}_p - \vec{k}_d| \geq 1.42$ fm^{-1}) at 800 MeV. Hints of this phenomenon are visible in the $T_p=185$ MeV data[21] where the 3^+ to 1^+ ratio is seen to grow from 1 to 1.7 as the laboratory scattering angle goes from 2.5° to 22.5° and the asymptotic momentum transfer increases from $q=0.72$ to 1.37 fm^{-1}. Recent measurements at TRIUMF (Ref. 22) indicate that for $T_p=200$ MeV the 3^+ to 1^+ ratio is about unity at forward angles ($\theta \sim 12°$ or $q \sim 1.0$ fm^{-1}). At $T_p=400$ MeV (Ref. 22) the 3^+ to 1^+ ratio is about 4 at all angles ($15° \lesssim \theta \lesssim 45°$ or 1.6 fm$^{-1} \lesssim q \lesssim 3.6$ fm^{-1}).

No attempt was made to extract peak areas for the broad region of excitation at 5.5 MeV, but its strength appears to have grown with energy relative to the ground state in roughly the same proportion as the 3^+ level. This region contains 2^+ $T=1$ and 1^+ $T=0$ levels and, while they do not both have "high" spins relative to the ground state, the wave functions of Norton and Goldhammer[23] suggest that they have predominantly $L=2$ spatial configurations like the 3^+ level, as opposed to the $L=0$ configuration of the ground state.

The only other level with a spatial configuration like the ground state is the 3.56 MeV 0^+ $T=1$ level. At lower energies [($T_p < 185$ MeV) (Ref. 21)] this level is excited with roughly one-half the strength of the ground state, a finding consistent with calculated spectroscopic factors[19,23] for these levels. At $T_p=800$ MeV the 3.56 MeV state is not observed and the upper limit for the cross section seems to be substantially less than one-half of the ground state value. Finally, the 4.31 MeV 2^+ $T=0$ level is weakly excited, if at all, at lower energies and is not seen here.

C. ^{12}C(p,d)^{11}C

A spectrum for the ^{12}C(p,d)^{11}C reaction taken at a laboratory angle of 19° is displayed in Fig. 2 and, as with all nuclei discussed here, a list of the known levels excited appears in Table I. The strong, well-defined peaks with excitation energies below 9 MeV of excitation are all well known from the many previous measurements at low energies. The lowest 10 MeV of excitation in the present spectrum is also very similar to the published $T_p=700$ MeV measurements of Baker *et al.*[1] which extend only to

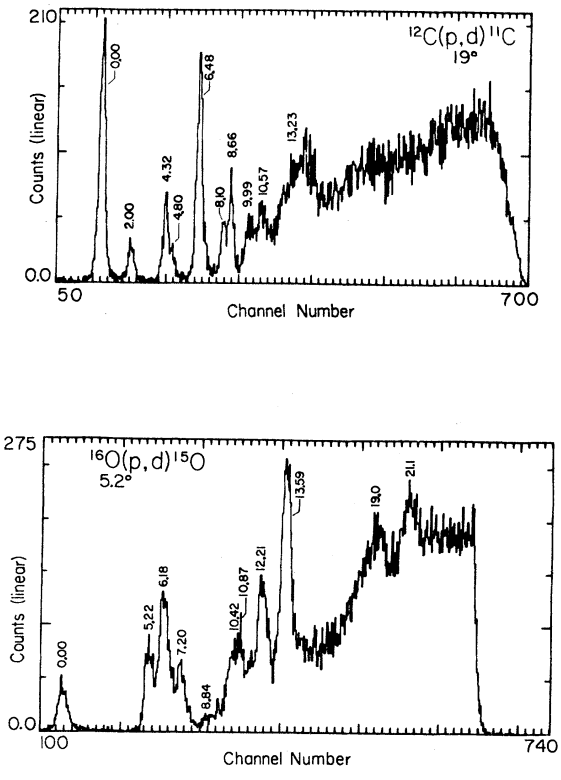

FIG. 2. Spectra for the (p,d) reaction on ^{12}C and ^{16}O are shown.

about that excitation. The relative strengths with which the well-known levels are populated is quite different from what is observed at lower energies.[19,20,24–31] While the relative strengths of the low-spin single-hole levels—namely the $\frac{3}{2}^-$ ground state, the 4.80 MeV $\frac{3}{2}^-$ level, and the 2.00 MeV $\frac{1}{2}^-$ level—are roughly the same as at lower energies, the high spin levels—such as the 4.32 MeV $\frac{5}{2}^-$ and 6.48 MeV $\frac{7}{2}^-$ levels—have grown in cross section relative to the ground state by at least a factor of 2. This phenomenon was explored in some detail by Källne and Obst[13] who interpreted it as an indication of the increased importance of multistep reaction pathways in exciting high spin levels at intermediate energies. This conclusion is entirely supported by lower energy studies[31–33] which indicate that direct single-step excitation of the first $\frac{5}{2}^-$ and $\frac{7}{2}^-$ levels in the ^{12}C(p,d)^{11}C reaction is negligible compared to multistep modes. Furthermore, as will be demonstrated in Sec. IV, coupled-channels Born approximation (CCBA) calculations using nuclear structure parameters which give excellent agreement for the lower energy $\frac{5}{2}^-$ and $\frac{7}{2}^-$ cross sections describe qualitatively the present 800 MeV data as well.

The most distinctive feature of the $T_p=800$ MeV ^{12}C(p,d)^{11}C spectra is the 2 MeV wide region of enhancement near an excitation energy of 13.2 MeV. This peak (or, possibly, group of peaks) is not observed in any lower energy measurements and yet is the strongest structure observed here. The excitation energy of the peak suggests that these high spin levels might be single-hole states based on the 14.08 MeV 4^+ level of ^{12}C just as the first $\frac{5}{2}^-$ and $\frac{7}{2}^-$ levels of ^{11}C are based on the 4.44 MeV 2^+ level of ^{12}C. The nuclear structure calculations of Norton and Goldhammer[23] also predict $\frac{9}{2}^-$ and $\frac{7}{2}^-$ levels in the vicinity of 13.2 MeV of excitation in ^{11}C with parentage based largely on the 4^+ in ^{12}C.

If conventional (i.e., "low energy") reaction modes are assumed, such an interpretation of the level or levels at 13.2 MeV requires that their excitation proceed through three distinct steps. This can be most readily understood by remembering that the inelastic excitation of the 14.08 MeV 4^+ level in ^{12}C proceeds through the 4.44 MeV 2^+ level via two steps. A third pickup step is then required to reach single hole states based on the 4^+. It should be noted that the 4^+ level in ^{12}C is roughly as strong as the 4.44 MeV 2^+ level in both intermediate energy proton inelastic scattering at back angles[35–37] and in the $T_p=800$ MeV ^{13}C(p,d)^{12}C reaction to be discussed below. This suggests that levels based on either the 2^+ or 4^+ levels should be of roughly equal strength even though two steps are involved in the former excitations and three in the latter. The observed relative strengths of the 13.2 MeV peak and the first $\frac{3}{2}^-$ and $\frac{7}{2}^-$ levels are consistent with this picture. These speculations about the structure of the 13.2 MeV level (or levels) will be discussed further in connection with CCBA calculations to be presented in Sec. IV.

D. ^{13}C(p,d)^{12}C

A sample spectrum for the ^{13}C(p,d)^{12}C reaction is displayed in Fig. 1. All of the strong positive parity states known to be formed by $1p$ pickup from lower energy studies are observed here (see Table I). The 7.66 MeV 0^+ and 9.64 MeV 3^- transitions which are very weak at lower energies are also very feeble at $T_p=800$ MeV. The relative strengths of the known $1p$ pickup states are essentially the same as at lower energies[27,38–41] with one important exception: the 0^+ ground state is only one-tenth as strong relative to the other levels at $T_p=800$ MeV. This again indicates preferential population of higher spin states. Furthermore, inspection of the L-S wave functions of Norton and Goldhammer[23] for $A=12$ show that, of all the strong pickup levels, the only one with an appreciable $L=0$ spatial component is the ground state where $L=0$ dominates; this may be another manifestation of the trend first discussed for ^{7}Li(p,d) above.

The $T_p=800$ MeV spectrum is remarkable in comparison to low energy measurements for other reasons as well. For instance, the 14.08 MeV level is excited just as strongly as the 4.44 MeV level—the strongest $1p$ pickup level—at 800 MeV, while at lower energies[38–42] no trace of this state is observed.

Although the spectrum of ^{12}C levels above 19 MeV is greatly obscured by ^{11}C states arising from ^{12}C contamination in the target, two strong previously unobserved levels can be identified at 20.6 and 25.4 MeV of excitation. To ensure that the 25.4 MeV level was not just an effect arising from the focal plane edge, spectra were accumulated at some angles for which the spectrometer momentum was adjusted to place the 25.4 MeV peak in the center of the focal plane. The $T_p=62$ MeV measurements of Parish *et al.*[27] show no indication of the 20.6 MeV level (their spectrum does not extend up to 25.4 MeV) and yet, in the present spectrum, it is roughly as large as the strongest lower level, the 4.44 MeV 2^+ state. The 25.4 MeV level is stronger still, by far the largest peak in the spectrum. While there is no information as to the spin and parity of the 25.4 MeV level, it is possible that the 20.6 MeV level may be either one or two 3^+ levels, either a $T=0$ or a $T=0$ and a $T=1$.[34] Such a state (or states) might be expected to behave similarly to the 14.08 MeV 4^+ level in that it would have a relatively high spin and could not be reached directly via a single $1p$ pickup step.

E. ^{16}O(p,d)^{15}O

A spectrum measured for the ^{16}O(p,d)^{15}O reaction at a laboratory scattering angle of 5.2° is shown in Fig. 2. At lower energies[19,20,28,29,42–44] the spectrum for this reaction is dominated by the two strong single-hole states, the $\frac{1}{2}^-$ ground state and 6.18 MeV $\frac{3}{2}^-$ level. Both transitions are observed here, but in the present case the $\frac{3}{2}^-$ level is preferentially populated, having roughly three times the strength of the $\frac{1}{2}^-$ ground state, while at lower energies their strengths are nearly equal.

The $T_p=800$ MeV spectrum is even more sharply distinguished from its lower energy counterparts by the presence of many strong peaks in addition to those to the first $\frac{1}{2}^-$ and $\frac{3}{2}^-$ levels. Several of these peaks are stronger than either of the strong single-hole states. For example, the 5.18 MeV $\frac{1}{2}^+$-5.24 MeV $\frac{5}{2}^+$ doublet has roughly $\frac{1}{10}$

of the strength of the ground state in the (p,d) reaction at $T_p=45$ MeV,[42] while it is equal in strength to the ground state at the present energy. Likewise, the 7.28 MeV $\frac{7}{2}^+$-7.56 MeV $\frac{1}{2}^+$ doublet grows by about the same factor relative to the ground state over the same energy range. Possible multistep mechanisms for these higher spin states are treated in Sec. IV.

As found for the carbon targets, broad but strong peaks are found at higher excitation in ^{15}O. Their excitation energies are listed in Table I.

F. ^{25}Mg(p,d)^{24}Mg

Many discrete levels are observed in the ^{25}Mg(p,d)^{24}Mg reaction. A spectrum acquired at a laboratory scattering angle of 5.2° is displayed in Fig. 3. For this target, the $T_p=800$ MeV spectrum is not qualitatively different from that which is observed at lower energies, e.g., in the ^{25}Mg(^{3}He,α)^{24}Mg reaction at $T_{^3\mathrm{He}}=18$ MeV.[45] In fact, the levels seen in the present work at 7.66, 8.36, 9.44, 10.63, 11.05, and 11.99 MeV can be identified with strong states of relatively high spin populated by this reaction.[45] The 10.12 MeV level seen in the present work can possibly be identified with the known 5^- level at 10.026 MeV which would not be populated in a simple one-step pickup process and is not observed in the (^{3}He,α) measurements. These correspondences are listed in Table II.

The relative strengths of the first three peaks in the present work differ appreciably from what is observed in lower energy neutron pickup reactions.[45–47] Here, the ratios of the 0^+ ground state, 2^+ 1.37, and 4^+-2^+ 4.12 MeV peaks are roughly 1:5:6 while low energy measurements give about 1:25:1, again indicating the preferential population of high spin states.

G. ^{28}Si(p,d)^{27}Si

Figure 3 shows a spectrum for the ^{28}Si(p,d)^{27}Si reaction taken at a laboratory angle of 12.5°. As with most of the nuclei discussed previously, the present spectra are quite different from those observed for lower energy neutron pickup reactions.[20,28,30,48–54] The $\frac{5}{2}^+$ ^{27}Si ground state dominates the spectrum at lower energies while there are many larger peaks in the spectra shown in Fig. 3, especially at excitation energies of 7.18 MeV and above. Closer examination of the spectrum shows that the ground state is weaker relative to nearly all other peaks. Even the 0.80 MeV group consisting of a $\frac{1}{2}^+$-$\frac{3}{2}^+$ doublet is appreciably stronger than at lower energies[20,28,49,52,54] indicating that high spin cannot be the sole factor contributing to the unusual level population seen in the present measurements.

There are some lower energy results which do suggest that several of the strongest peaks seen in the $T_p=800$ MeV spectra are associated with high spin levels. The

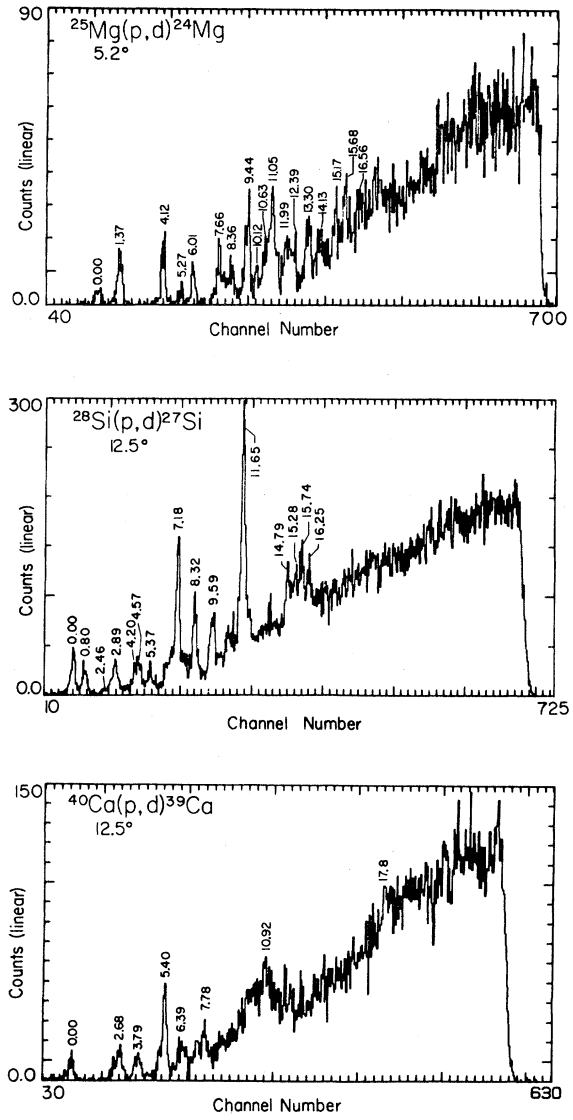

FIG. 3. Neutron pickup spectra for targets of ^{25}Mg, ^{28}Si, and ^{40}Ca are shown for 800 MeV protons.

TABLE II. ^{25}Mg(p,d)^{24}Mg: Correspondences with known levels in ^{24}Mg.

Present work	(^{3}He,α) (Ref. 45)	Endt and van der Leun (Ref. 55)	
E_x	E_x	E_x	J^π,T
7.66	7.610	7.6162	$3^-,0$
	8.367	8.3579	$3^-,0$
8.36			
	8.446	8.4362	$4^+,0$
9.44	9.452	9.4558	$3^+,0$
		10.026	$5^-,0$
10.12	10.07	10.059	$2^+,1$
	10.163	10.161	
11.05	11.022	11.018	$2^+,0$
		11.9304	
11.99	11.939	11.9859	2^+
		12.0144	$3^-,0$
		12.0486	$4^+,0$

$T_{^3He}=216$ MeV $^{28}Si(^3He,\alpha)^{27}Si$ measurements of Refs. 52 and 53 show that a peak corresponding to the 2.16 MeV $\frac{7}{2}^+$ level and another unidentified one at 7.15 MeV grow markedly relative to the ground state as the scattering angle increases. Van de Wiele *et al.*[53] argue that the $\frac{7}{2}^+$ level is probably populated via a two-step process consisting of inelastic excitation of the 1.78 MeV 2^+ level of ^{28}Si followed by $1d_{5/2}$ pickup. By analogy, they argue that the 7.15 MeV level is excited by a similar process and that it has a spin and parity of $\frac{7}{2}^+ \leq J^\pi \leq \frac{11}{2}^+$. While such a level is not known in ^{27}Si, a 7.17 MeV $\frac{9}{2}^+$ level is tabulated for the mirror nucleus, ^{27}Al. No excitation is observed at 2.16 MeV in the present work but a very strong excitation is observed at 7.18 MeV and the uncertainty associated with the extracted excitation energy permits correspondence with the 7.15 MeV level of Van de Wiele *et al.*[53] This finding then appears to be consistent with their assignment of high spin, though perhaps not with their speculation as to the structure of the level.

The $T_p=136$ MeV $^{28}Si(p,d)^{27}Si$ measurements of Miller *et al.*[51] are even more suggestive. The angular distribution for the 2.16 MeV $\frac{7}{2}^+$ level is observed to be much flatter than for the strong single-hole levels such as the $\frac{5}{2}^+$ ground state. Miller *et al.* take this flatness to be a signature of two-step excitation processes and use this feature to identify tentatively other high spin levels. Several of these correspond to strong peaks observed in the present work. Specifically, their tentative high spin states at 7.12, 8.37, 9.62, and 11.65 MeV correspond, within experimental uncertainties, to the levels observed here at 7.18, 8.32, 9.59, and 11.65 MeV, respectively. The relatively flat angular distribution observed for these levels at $T_p=136$ MeV show broad maxima at varying angles and while they do not permit firm angular momentum assignments, the locations of these maxima can be interpreted using simple kinematic arguments to give approximate J values for the final states. This is done by assuming that the maximum occurs at the angle for which the classical angular momentum transfer corresponds to the J value of the final state. Quantitatively the relation is

$$q(\theta)R \sim J ,$$

where $q(\theta)$ is the (angle-dependent) momentum transfer and R is an interaction radius, determined in this case by noting that the 2.16 MeV $\frac{7}{2}^+$ level has a maximum at $\theta_{c.m.}\sim 20°$ or $q\sim 245$ MeV/c. These numbers give $R=2.8$ fm. The following rough spin assignments were made: 7.12 MeV, $J=\frac{9}{2}, \frac{11}{2}$; 8.37 MeV, $J=\frac{7}{2}, \frac{9}{2}$; 9.62 MeV, $J=\frac{7}{2}$; 11.65 MeV, $J=\frac{9}{2}, \frac{11}{2}$. Note that the spin of the 7.12 MeV level determined in this manner is consistent with the identification of this level as the mirror of the 7.17 MeV $\frac{9}{2}^+$ level in ^{27}Al suggested in the preceding paragraph.

A possible parentage for the strong levels in the present work at and above 7.18 MeV of excitation has been suggested by Miller[56] who noted an interesting correlation between these levels and the high-spin negative-parity states strongly excited in inelastic scattering on ^{28}Si. This correspondence is presented graphically in Fig. 4 and indicates that the strong ^{27}Si levels might be formed by coupling a $1d_{5/2}$ neutron hole to the states in ^{28}Si. This would, of course, give rise to negative parity levels. It should be noted that a $\frac{9}{2}^-$ level is tabulated[55] for ^{27}Al at an excitation energy of 7.23 MeV, again within the uncertainty of the 7.18 MeV excitation energy determined in the present work. The correspondences of Fig. 4 are also consistent with all of the rough spin determinations made in the preceding paragraph. Note also that the strongest level seen at 11.65 MeV is associated with the level of highest spin, the 11.58 MeV 6^- $T=0$ state, in ^{28}Si.

This description may account for the very different strengths of the 2.16 MeV $\frac{7}{2}^+$ level—which is not observed—and the 7.18 MeV level which Van de Wiele *et al.*[53] suggested have the same parentage based on the first 2^+ level of ^{28}Si. Simple energy considerations suggest that the $\frac{9}{2}^+$ level at 2.91 MeV be identified as the $\frac{9}{2}^+$ member of the weak coupling multiplet based on this 2^+ level, not the $\frac{9}{2}^+$ level at 7.17 MeV (in ^{27}Al). This lower $\frac{9}{2}^+$ state must contribute to the 2.89 MeV peak where it is not resolved from the $(\frac{3}{2},\frac{5}{2})^+$ level at 2.87 MeV. The 2.89 MeV peak shows no significant enhancement at the present energy relative to the 0.80 MeV peak which has no high spin components. This is consistent with little or no enhancement of the high spin 2.91 MeV level which is, in turn, consistent with weak excitation of the 2.16 MeV $\frac{7}{2}^+$ level if the latter two levels are assumed to have the same structure. A strong preference for two step modes to proceed through the higher spin negative parity levels of ^{28}Si rather than the 2^+ would then account for the differential population of the 2.16 MeV $\frac{7}{2}^+$ and 7.18 MeV levels if the latter were based on the 6.88

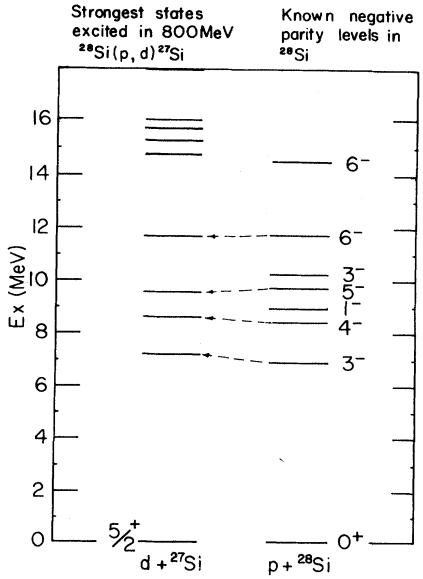

FIG. 4. Correspondences between negative parity levels of ^{28}Si and the strongest states excited in the 800 MeV $^{28}Si(p,d)^{27}Si$ reaction suggesting an interpretation of these latter levels based on a weak coupling model. (See the text.) Several negative parity levels of ^{28}Si between 12 and 14 MeV have been omitted for clarity.

MeV 3^- level as suggested in Fig. 4. It would be very interesting to test these speculative notions with low energy spectroscopic measurements.

There is a broad (2 MeV) region of excitation observed in the present measurements at about 15.5 MeV, which is reminiscent of that observed at 13.2 MeV in the $^{12}C(p,d)^{11}C$ reaction and at 19 and 21 MeV in the $^{16}O(p,d)^{15}O$ reaction. For $^{28}Si(p,d)^{27}Si$, however, this broad peak was observed to resolve itself into four distinct peaks at some angles as shown in Fig. 3. As for the other targets, no such structures are observed in the lower energy measurements[28,52,53] and no correspondence with previously known levels can be made.

H. $^{40}Ca(p,d)^{39}Ca$

The heaviest of the targets considered in the present study is ^{40}Ca. A spectrum for the $^{40}Ca(p,d)^{39}Ca$ reaction at a laboratory scattering angle of 12.5° is displayed in Fig. 3. Very few levels in ^{39}Ca are unambiguously known above 3.03 MeV of excitation. This fact, coupled with the high level density of ^{39}Ca and the relatively poor excitation energy determinations possible for the present measurements, allows only the $\frac{3}{2}^+$ ground state peak to be identified with certainty. The peak at 2.68 MeV of excitation probably contains contributions from the 2.47 MeV $\frac{1}{2}^+$, 2.80 MeV $\frac{7}{2}^-$, and 3.03 MeV $\frac{3}{2}^-$ levels. Low energy single nucleon pickup measurements leading to ^{39}Ca or its mirror, ^{39}K, show strong single hole strength for the ground state, 2.47 MeV $\frac{1}{2}^+$, and 2.80 MeV $\frac{7}{2}^-$ levels as well as states at 5.13, 5.49, and 6.16 MeV thought to be populated by $1d_{5/2}$ pickup.[57] As for the other targets discussed above, the relative state populations observed in the present work are quite different from those at lower energies.[20,29,44,49,57–61] In the latter measurements, each of the strong single-hole states mentioned above possesses typically 20% to 70% as much strength as the ground state, while in the present study the peaks at 2.68, 3.79, and 5.40 MeV are two to four times stronger than the ground state. This difference cannot be accounted for by the poorer resolution of the present measurements lumping contributions from adjacent strong single-hole levels. The difference in relative population is greatest for the 3.79 MeV peak. At low energies[20] the total strength in the region from 3.6 to 4.0 MeV of excitation is less than 20% of the ground state while it is about 60% stronger than the ground state here. Again it is tempting to ascribe this effect to enhanced excitation of high spin levels in the intermediate energy (p,d) reaction. In the mirror nucleus ^{39}K there are high spin states in this region—a 3.60 MeV $\frac{9}{2}^-$ and a 3.94 MeV $\frac{11}{2}^-$ level[55]—which are likely to arise from a $1d_{5/2}$ or $1d_{3/2}$ hole coupled to either the 3.74 MeV 3^- or 4.49 MeV 5^- levels of ^{40}Ca, both of which are strongly collective.

Another remarkable feature of the spectrum of Fig. 3 is the presence of two broad (again, 2 MeV) regions of excitation at roughly 11 and 18 MeV which contain most of the discrete strength observed in this reaction. These structures are similar to ones noted above for the ^{12}C, ^{16}O, and ^{28}Si (p,d) reactions. No such strength is observed at lower energies.[29,49]

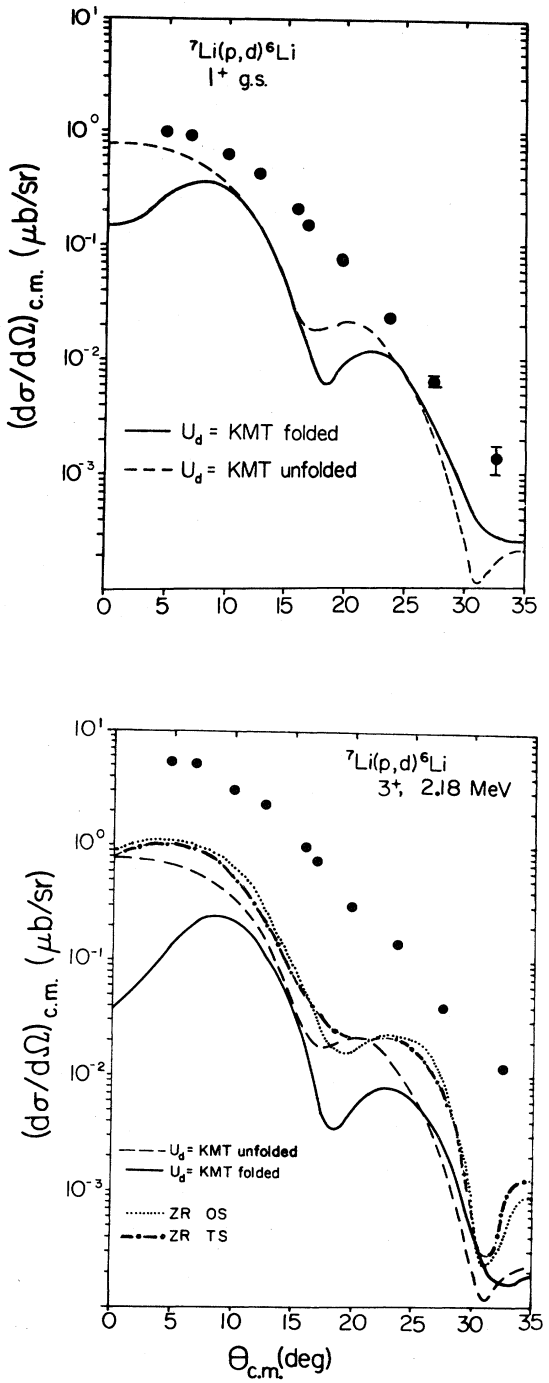

FIG. 5. Data for the 800 MeV $^7Li(p,d)^6Li$ (1^+ g.s.) reaction are shown and compared with EFR DWBA calculations using folded and unfolded KMT deuteron potentials (see the text) and $\Sigma C^2S = 0.83$. Data for the $^7Li(p,d)^6Li$(2.18 MeV 3^+) reaction are compared with EFR DWBA calculations using folded and unfolded KMT deuteron potentials and $C^2S = 0.47$. Also shown are ZR one-step (OS) and two-step (TS) CCBA calculations. The latter include inelastic excitations in the proton channel with coupling strengths given by the rotational model. The difference between the OS and TS calculations is seen to be small compared with the discrepancy with the data.

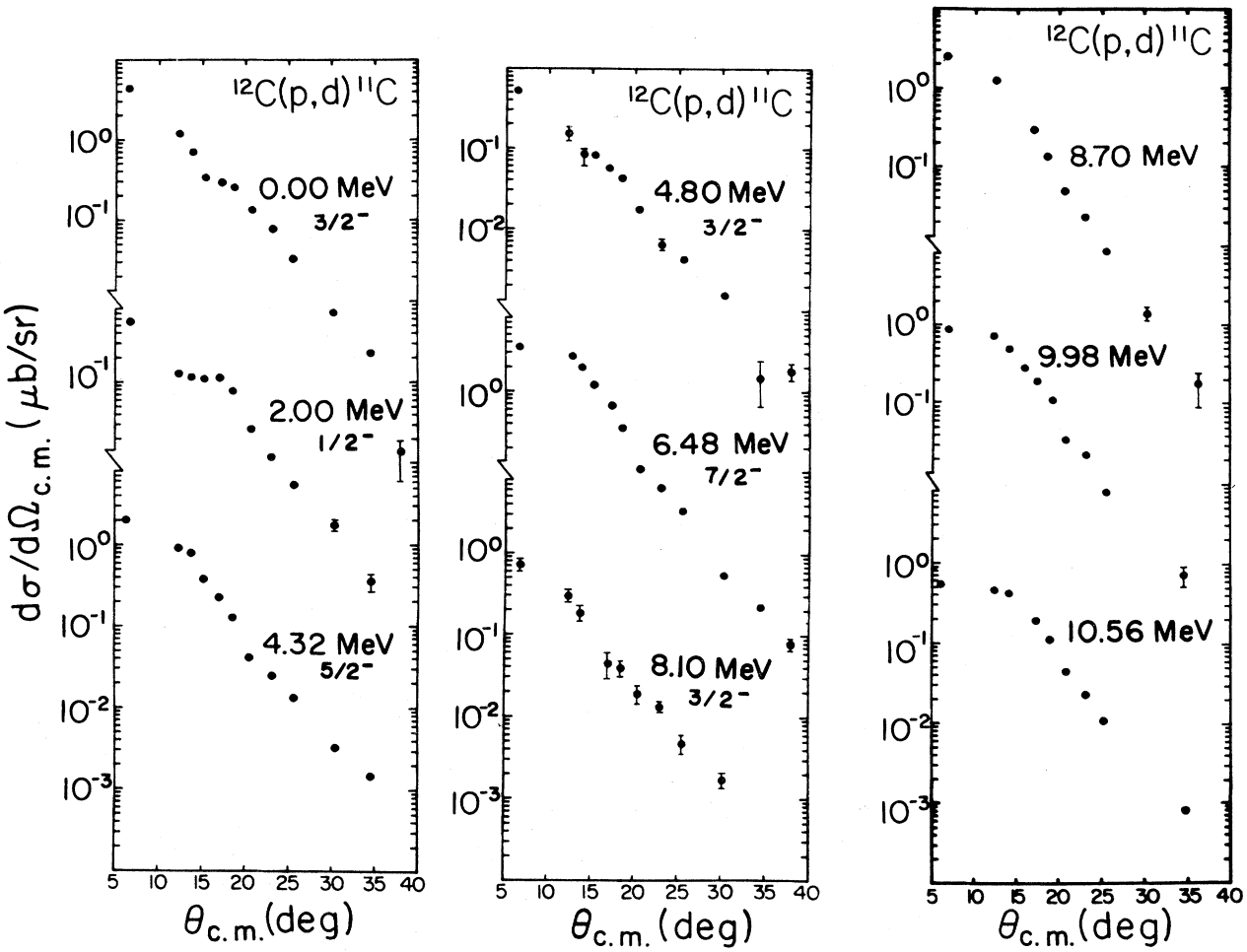

FIG. 6. Angular distributions observed for known and newly seen states in ^{11}C are shown for the 800 MeV (p,d) reaction.

I. Angular distributions

Angular distributions for transitions to the lowest levels of the nuclei studied are presented in Figs. 5—8. Those corresponding to highly excited final states are also presented for the $^{12}C(p,d)^{11}C$ reaction. The most striking feature of these angular distributions is their similarity, all possessing an essentially featureless monotonic decrease as a function of scattering angle. This situation is in sharp contrast to that observed at lower energies where angular distributions can vary tremendously depending on the orbital angular momentum transfer. In the present work, however, no such strong dependence appears. Angular distributions arising from $1p$ pickup such as those of the $^{7}Li(p,d)^{6}Li$ reaction (Fig. 5) have essentially the same shape as those involving $1d$ pickup, such as the ground state transitions in the ^{28}Si and ^{40}Ca (p,d) reactions (Fig. 8). At low energies the shapes of angular distributions generally depend quite strongly on the number of steps involved in the excitation process. In the low energy $^{12}C(p,d)^{11}C$ reaction,[13,25] for instance, the strong single particle transition to the $\frac{3}{2}^-$ ground state of ^{11}C gives rise to a very different angular distribution than does the principally two-step transition to the 4.32 MeV $\frac{5}{2}^-$ level, the latter being much flatter. In the present work, the corre-

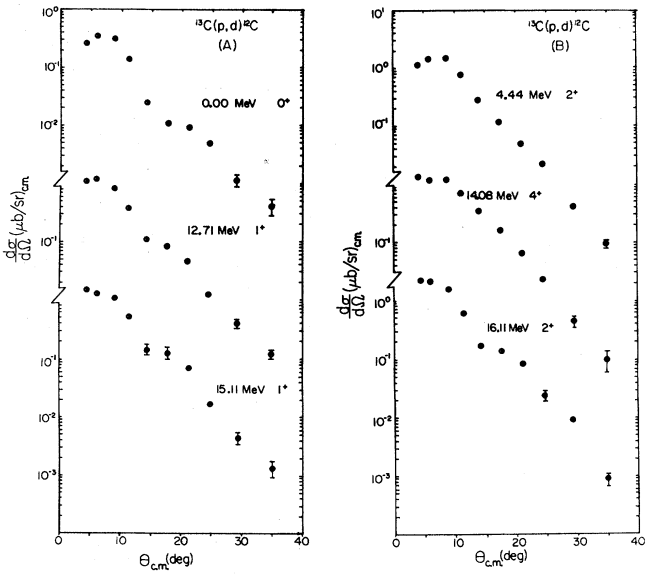

FIG. 7. The angular distributions observed for the known states of ^{12}C are shown.

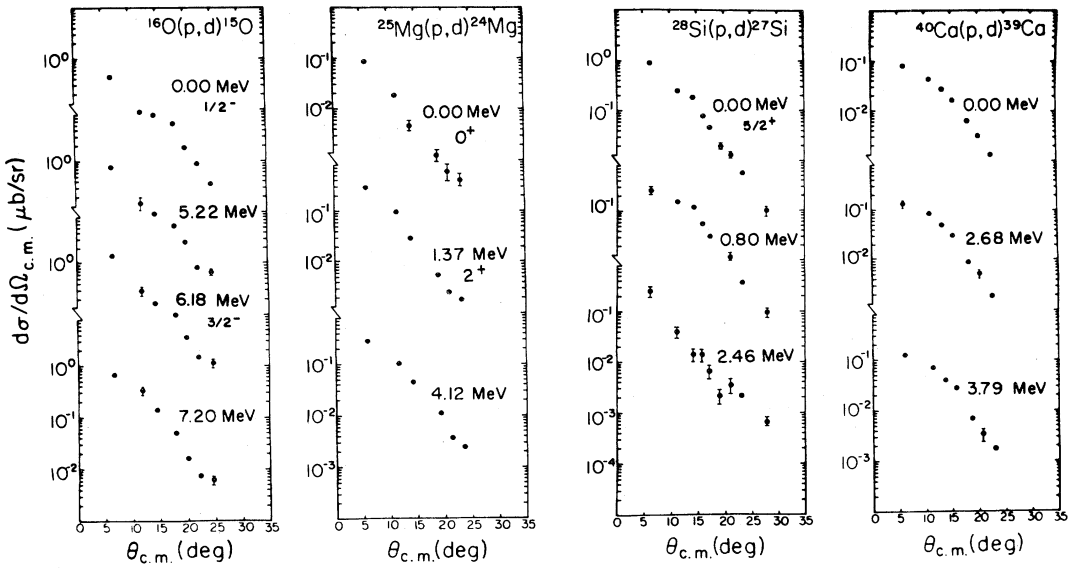

FIG. 8. Pickup data for states of ^{15}O, ^{24}Mg, ^{27}Si, and ^{39}Ca are shown.

sponding angular distributions are very similar, as is shown in Fig. 6.

In spite of the general similarity of the $T_p = 800$ MeV angular distributions, some systematic differences can be discerned at a detailed level. For instance, angular distributions for transitions to low-lying levels, especially when small angular momentum transfers are involved, show distinct inflection points. All ground state transitions, except those for the ^{7}Li and ^{40}Ca (p,d) reactions show this. The structure of the ^{13}C(p,d)^{12}C(0$^+$,g.s.) angular distribution (Fig. 7) is particularly pronounced.

Transitions to high-spin states which are likely to arise predominantly from multistep processes show virtually no structure in their angular distributions. The smooth, monotonic falloff observed for the 14.1 MeV 4$^+$ level of ^{12}C (Fig. 7) is characteristic of this effect. Such angular distributions are also frequently somewhat flattened in the forward angle region. Most of the angular distributions observed for transitions to high lying levels of unknown spin and parity have these characteristics, further supporting their identification as high spin states.

For all targets lighter than ^{40}Ca—except ^{7}Li and ^{25}Mg—typical $T_p = 800$ MeV (p,d) cross sections have roughly the same magnitude, independent of mass. (Nuclear structure effects tend to concentrate strength for ^{7}Li and spread it for ^{25}Mg.) For ^{40}Ca(p,d)^{39}Ca, typical cross sections abruptly drop by about an order of magnitude, the exception being for the broad 11 MeV peak. The origin of this effect is unknown.

IV. THE DWBA METHOD AND COMPARISON WITH DATA

A. The DWBA transition amplitude

The distorted wave Born approximaton (DWBA) has long been used to calculate (d,p) or (p,d) reaction amplitudes.[62] Implicit in this nonrelativistic approach is the assumption that the nucleons involved are fundamental particles and that the transferred neutron is picked up in a single step. In this section we outline the derivation of the standard DWBA amplitude for (p,d) in order to emphasize the approximations made and their physical implications at higher energy. The new regime of momentum transfer for the present data enables fresh tests of the assumptions in the standard DWBA method. Let us consider the reaction A(p,d)B. After some standard manipulations,[62] the exact transition amplitude can be written

$$T_{pd} = \langle \Psi_{dB}^{(-)} \mid V_{pn} + V_{pB} - U_p \mid (\phi_n \Phi_B)_A \chi_p^{(+)} \rangle \ , \qquad (1)$$

where $\Psi_{dB}^{(-)}$ is the total scattering solution corresponding to an asymptotic plane wave in the dB partition and only incoming spherical waves in the others, V_{pn} and V_{pB} are the proton-neutron and proton-core potentials, respectively, ϕ_n and Φ_B are the neutron bound state and core wave functions, respectively, and $\chi_p^{(+)}$ is an eigenfunction of the optical potential U_p with outgoing spherical waves. The choice of U_p is arbitrary but the philosophy of the DWBA is to choose it so that it cancels the effects arising from V_{pB}. Since V_{pB} and U_p are very different operators, V_{pB} depending on the coordinates of all target nucleons individually while U_p depends only on a single channel variable, the cancellation must be between the last two matrix elements of Eq. (1), not between V_{pB} and u_p themselves. The standard formulation of the (p,d) reaction then proceeds by assuming that no rearrangement of the core B occurs, the original $(A+1)$-body problem thereby becoming a three-body problem. This step provides some guidance in the choice of U_p. Since the $p + B$ scattering process not involving rearrangement of B is essentially elastic scattering, it is loosely argued that U_p should be the optical potential describing the $p + B$ elastic scattering. Implicit in this prescription is the reasonable assumption that any interaction of the incident proton with the constituents of B which takes the proton out of the $p + B$ elastic channel will also cause a diminished contribution to the pickup process.

The amplitude of Eq. (1) is then further simplified by assuming that $|\Psi_{dB}^{(-)}\rangle \simeq |\chi_{dB}^{(-)}\phi_d\rangle$, where $\chi_{dB}^{(-)}$ is a deuteron elastic scattering wave function generated from an optical potential U_d, and ϕ_d is the deuteron internal wave function. The justification of this step is similar to that given above for the proton channel[63] although some additional complications arise for the deuteron. These will be discussed below in some detail. The resulting (standard) DWBA amplitude is then

$$T_{dP}^{DWBA} = \langle \chi_d^{(-)} | V_{pn} | \phi_n \chi_p^{(+)} \rangle . \quad (2)$$

Some of the qualitative behavior of the DWBA transition amplitude can be interpreted by replacing the distorted waves, χ, of Eq. (2) by plane waves. In such a case, one obtains the plane wave Born approximation (PWBA), which has a very simple form, namely it is proportional to

$$\int d\vec{\rho}\, e^{i\vec{q}\cdot\vec{\rho}} V_{pn}(\vec{\rho})\phi_d(\vec{\rho}) \int d\vec{r}_{nB} e^{i\vec{Q}\cdot\vec{r}_{nB}} \phi_n(\vec{r}_{nB}) \equiv D(\vec{q})\tilde{\phi}_n(\vec{Q}) , \quad (3)$$

where ϕ_n is the wave function of the picked up neutron in ϕ_A,

$$\bar{r}_{nB} = \bar{r}_n - \bar{r}_B , \quad \bar{\rho} = \bar{r}_p - \bar{r}_n ,$$

$$\bar{q} \equiv \bar{k}_{pA} - \tfrac{1}{2}\bar{k}_{dB} , \quad (4)$$

and

$$\bar{Q} \equiv \frac{A-1}{A}\bar{k}_{pA} - \bar{k}_{dB} .$$

Thus the plane wave amplitude is the product of the Fourier transform of $V_{pn}\phi_d$, reflecting the reaction dynamics, and the Fourier transform of $\phi_n(Q)$ reflecting the nuclear structure aspects of the reaction. This leads to the hope that the high energy (p,d) reaction can map out the Fourier transform of the picked-up neutron to high values of q. This will be examined in Secs. IV B and IV C.

B. The deuteron wave function

In Fig. 9, the projectile Fourier transform $D(q)$ [Eq. (3)] is plotted versus q for two choices of the deuteron wave function, namely a Hulthén form and an eigenfunction of the Reid soft-core potential.[64] Also shown is the range of q contributing to T_{dp}^{PWBA} for various values of T_p. At low energies where q is very small, the simple Hulthén form is seen to be adequate since it is not appreciably different from the more realistic Reid soft-core wave function. At higher energies the D-state contribution, $D_2(q)$, is seen to become quite important, indeed dominant. Hence a simple S-state deuteron wave function is fundamentally insufficient, apart from the additional failure to reproduce the detailed behavior of $D_0(q)$ for large q.

The quantities displayed in Fig. 9 help us to understand several properties of the DWBA amplitude. The six-dimensional integral in Eq. (2) is usually reduced to a three-dimensional integral by making the zero range approximation, assuming $V_{pn}(\bar{\rho})\phi(\bar{\rho}) \sim D_0\delta(\bar{\rho})$, where $D_0 = D_0(q=0) = -125$ MeV fm$^{3/2}$. This is equivalent to

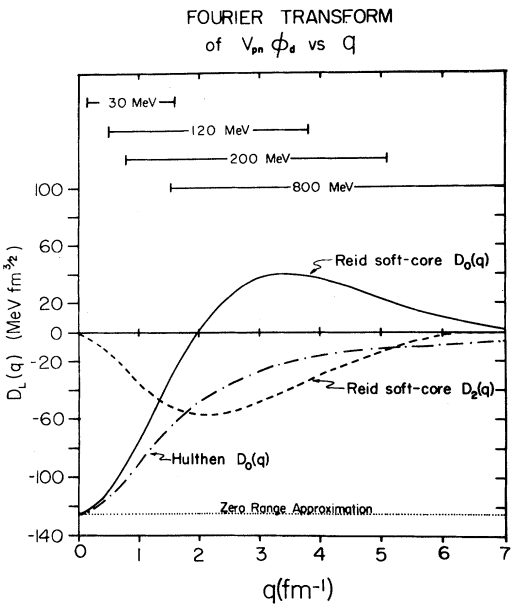

FIG. 9. The projectile Fourier transform of $V_{pn}\phi_d$ [See Eq. (4)] is shown for Hulthén and Reid soft-core deuteron wave functions. The effective D_0 implied by the zero-range approximation is indicated by the dotted line. The horizontal bars show the range of momentum sampled by the ^{12}C(p,d)^{11}C(g.s.) reaction at various energies assuming no distortion effects (PWBA).

assuming that $D_0(q)$ is a constant as indicated by the horizontal dotted line in Fig. 9. Such an approximation works quite well at low energies. A so-called "finite range correction"[62] to this approximation, which takes into account the curvature of $D_0(q)$ at $q=0$ but which still requires only the evaluation of a three-dimensional integral, improves low energy agreement. However, it is obvious from Fig. 9 that at intermediate energies, such approximate techniques are likely to be inadequate. In fact, it has been shown that in order to have absolutely normalized calculations the full six-dimensional integral in Eq. (2) must be evaluated for ^{12}C(p,d)^{11}C(g.s.) at $T_p = 700$ MeV (Ref. 10) and for the intermediate energy (p,d) reaction in general.[9-12] It is also clear from Fig. 9 that if the zero range approximation is retained, then the effective zero range normalization will be energy dependent, tending to decrease with increasing energy. This effect is also observed. In an analysis by Baker *et al.*[1] of the ^{12}C(p,d)^{11}C(g.s.) data at 700 MeV, an effective D_0 of -60 MeV fm$^{3/2}$ was required to normalize zero range calculations. This effective D_0 is roughly consistent with the value suggested by Fig. 9 based on a momentum transfer to the deuteron, $\bar{q} = \bar{k}_p - \frac{1}{2}k_d$, about 2 fm^{-1} at $T_p = 700$

C. The neutron bound state wave function

The second factor in the PWBA amplitude [Eq. (3)] is $\tilde{\phi}_n(\bar{Q})$, or the Fourier transform of the bound neutron in the target. The behavior of this quantity for low Q (< 1.5 fm^{-1}) is determined almost solely by its binding

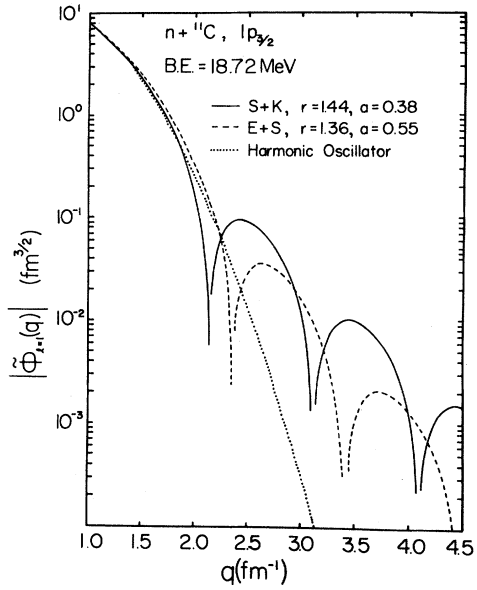

FIG. 10. The Fourier transform of various n + ^{11}C $1p_{3/2}$ wave functions is shown for $q \geq 1.0$ fm^{-1}. The transform of the eigenfunction of a Woods-Saxon well with Shepard and Kaczkowski geometry (Ref. 68) is compared with that of Elton and Swift (Ref. 65) and with that for a harmonic oscillator wave function having the same rms radius as the Shepard and Kaczkowski eigenfunction. Note that the 800 MeV ^{12}C(p,d)^{11}C reaction would sample these transforms at $q \geq 2$ fm^{-1} in the absence of distortions (PWBA).

energy and l and j values, while the radial (in momentum space) behavior is governed by simple size considerations. In fact, as Fig. 10 demonstrates, only slight differences are observed in this momentum range between harmonic oscillator wave functions and more realistic ones (e.g., eigenfunctions of a Woods-Saxon well), so long as both wave functions have the same rms radii. It is therefore not surprising that low energy (p,d) data where the relevant momentum transfers are less than 1.5 fm^{-1} can provide spectroscopic information (e.g., l and j values) but not detailed information about the radial wave function itself. Apart from detailed differences, all versions of $\tilde{\phi}_n(\bar{Q})$ drop quite rapidly as Q increases. This behavior explains, at least in part, why the (p,d) cross section drops so rapidly as T_p increases and, consequently, Q increases.

At a more detailed level, as Q increases beyond 1.5 fm^{-1}, significant differences between various types of theoretical neutron wave functions begin to appear. An example of this is shown in Fig. 10. These differences can arise from a number of sources, such as the details of the single particle well. Experimental determination of the high momentum behavior of single neutron wave functions would be very valuable and, based on the PWBA, seems feasible with the intermediate energy (p,d) reaction. (The extent to which distortion effects hinder such determinations will be addressed in detail below.)

With this in mind, single neutron wave functions in the present work have been generated according to a prescription similar to that typically used in low energy analyses but with the additional constraint that there be consistency with large q elastic electron scattering data. Specifically, the single neutron wave functions are taken to be the eigenfunctions (with appropriate nlj quantum numbers) of Woods-Saxon central and spin-orbit potentials, the strengths of which are adjusted to give the proper neutron separation energies. In the present prescription, the geometries of the Woods-Saxon wells are fixed for a given target nucleus by requiring that the charge density for that nucleus generated from its single particle proton wave functions be consistent with large q elastic electron scattering data for that nucleus. The details of the procedure and its similarity to and differences from other approaches,[65–67] such as that of Elton and Swift,[65] are discussed in Ref. 68. The sensitivity of the procedure is illustrated in Fig. 11 where data[69] for ^{16}O elastic electron scattering are compared with calculations utilizing various radius and diffuseness values for the Woods-Saxon well binding the protons. Radius and diffuseness values determined in this way are listed in Table III.

It should be noted that this prescription is neither complete nor unique in its treatment of the relevant nuclear structure physics and that it also suffers from internal inconsistencies.[65–68] However, it does represent a reasonable first step in incorporating the high momentum infor-

TABLE III. Neutron bound state potentials for g.s.→g.s. transitions.

Nucleus	V (MeV)[a]	r_0 (fm)	a (fm)	λ[b]
^{7}Li	−39.3	1.82	0.55	0.0
^{12}C	−50.8	1.44	0.38	25.0
^{13}C[c]	−33.74	1.44	0.38	25.0
^{16}O	−47.20	1.44	0.55	25.0
^{25}Si	−55.99	1.33	0.70	25.0
^{40}Ca	−51.12	1.33	0.70	25.0

[a]Depth adjusted to give correct separation energy.
[b]Thomas spin orbit term, i.e.,

$$V_{SO} = \frac{-\lambda}{45.2}\frac{1}{r}\frac{dV(r)}{dr}\vec{L}\cdot\vec{S}\,.$$

[c]Reference 68.

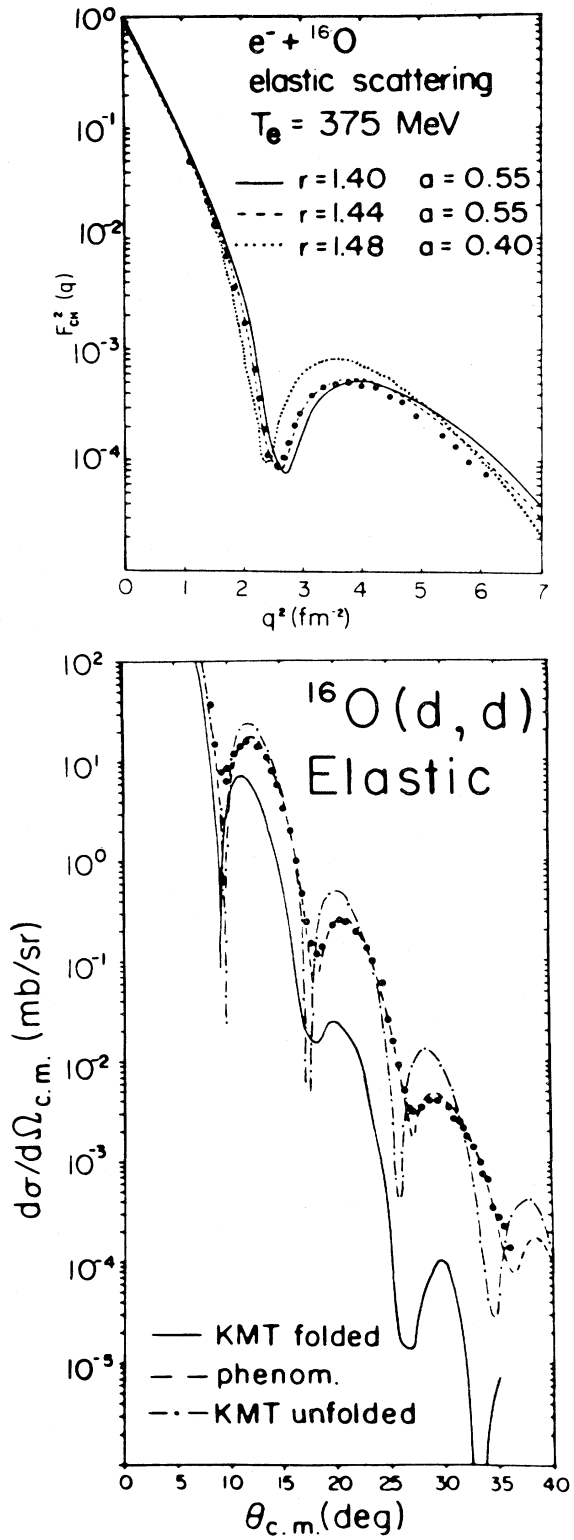

FIG. 11. The top portion shows the form factor for elastic electron scattering from ^{16}O compared to predictions using several geometrical parameter sets for the Woods-Saxon potential binding the protons. Below are shown elastic deuteron scattering data compared to predictions for several sets of optical model parameters. The phenomenological curve is the result of a best fit to the data. These parameters are listed in Table IV.

mation available in elastic electron scattering data in the single particle wave functions.

D. Proton and deuteron distorted waves

It is well known that at low energies careful treatment of proton and deuteron distortions is crucial for achieving quantitative agreement between experiment and the simple pickup theory. This is also true at intermediate energies. For example, Rost *et al.*[11] have shown that there are large differences between PWBA and DWBA calculations of ^{4}He(p,d)^{3}He(g.s.) cross sections for $T_p = 770$ MeV. Distortion effects are even greater for heavier targets.

As stressed above in the present version of the DWBA, distortions are generated using optical potentials which describe the interaction of the projectile with the core without causing rearrangement of the core and leads directly to the optical model potential which describes elastic scattering. Specific potentials can be obtained either theoretically [for example, using the Kerman, McManus, and Thaler (KMT) multiple scattering theory[70,71]] or phenomenologically by fitting relevant elastic scattering data. At the level of precision relevant in the present work, these two procedures give nearly identical results. The DWBA calculations to be presented below use phenomenological proton potentials obtained by fitting $T_p = 800$ MeV p + ^{12}C, ^{13}C,[35,36] and ^{58}Ni (Ref. 35) elastic scattering data. A standard optical model search program,[72] modified to include relativistic kinematics consistent with the DWBA codes to be discussed below, was employed in the fitting procedure. The potentials are presented in Table IV.

The choice of distorting potentials is not so clear-cut for the deuteron-core channel. For instance, it has been argued[73] that the most obvious choice for a distorting potential—a phenomenological one determined by fitting elastic scattering data—is inappropriate because it does not adequately account for deuteron breakup processes which can contribute to the (p,d) process and which cannot be treated explicitly in a two-body formulation. Similar objections have been lodged against the simplest of the folding model potentials—that of Watanabe[74]—which is obtained by folding the appropriate nucleon-nucleus potentials over the deuteron and which, by construction, is the lowest order theoretical representation of the phenomenological potential. At lower energies, improvements upon these potentials can be made relatively easily by using the Johnson-Soper two-body potential[73,75–77] which accounts for breakup effects approximately. It should be noted, however, that the theoretical justification of the Johnson-Soper prescription breaks down at intermediate energies due to the increased importance of finite-range effects and the presence of large proton-neutron relative momenta in the breakup channels.

One solution to these problems would be to treat the three-body deuteron-core problem explicitly. This has been done at lower energies by a number of investigators.[75,76,78,79] Such calculations are prodigious numerical undertakings and extending them to intermediate energies would increase their complexity enormously.

In the present work, two-body deuteron-core potentials

TABLE IV. Proton and deuteron optical model potentials for $T_p=800$ MeV A(p,d)B reaction. $U(v)=Vf_R(r)+iWf_I(r)$, $f_x(r)=\{1+\exp[(r-r_xA_x^{1/3})/a_x]\}^{-1}$. All depths in MeV and lengths in fm.

Potential	V	r_R	a_R	W	r_I	a_I
p + ^{12}C phenomenological	+13.73	0.872	0.304	−68.93	0.948	0.472
p + ^{58}Ni phenomenological	+2.97	1.100	0.537	−108.62	0.933	0.634
d + ^{6}Li	−9.70	0.946	0.734	−40.52	0.946	0.734
d + ^{11}C	−14.02	0.896	0.725	−58.64	0.896	0.725
d + ^{12}C	−15.70	0.856	0.727	−65.70	0.856	0.727
unfolded	−16.17	1.035	0.513	−67.65	1.035	0.513
d + ^{15}O folded	−16.02	0.910	0.767	−67.02	0.910	0.767
phenomenological	0			−75.85	0.96	0.537
d + ^{27}Si	−15.44	0.945	0.795	−64.62	0.945	0.795
d + ^{39}Ca	−16.20	0.970	0.801	−67.76	0.970	0.801

have been used to generate χ_d for use in DWBA calculations. Because of a nearly total lack of appropriate deuteron elastic scattering data, phenomenological potentials are not generally available. One kind of theoretical potential is the Watanabe-type discussed above, for which nucleon-nucleus potentials are folded over the deuteron density. As used in the present work, the deuteron density was taken to be that given by a Hulthén wave function with $\alpha=0.23$ fm^{-1} and $\beta=7\alpha$ in the proton-neutron relative coordinate. The other type of potential is generated according to the Johnson-Soper prescription—nucleon-nucleus potentials are combined without folding. The effects of using these different types of potentials on DWBA results will be addressed in detail below.

The nucleon-nucleus potentials used in generating the deuteron potentials were in turn constructed theoretically using the first term of the KMT multiple scattering series.[70,71] The nucleon-nucleon (NN) forward scattering amplitudes used were based on NN total cross-section measurements[80] and real-to-imaginary ratios were determined from tabulated NN phase shifts.[81] Nuclear densities were taken from a tabulation of elastic electron scattering results.[82] The details of the construction of the deuteron optical potentials are presented in their totality in Ref. 83. The potential parameters appear in Table IV.

One relevant deuteron elastic scattering data set does exist, for d + ^{16}O at $T_d=700$ MeV,[4] and best-fit parameters have been determined as part of the present work. They are presented in Table IV. The best fit elastic scattering calculations are compared with data and with calculations using the folded and unfolded theoretical potentials in Fig. 11. Numerically the imaginary parts of all three potentials are very similar. The small real potential has virtually no influence on the calculated cross sections and was arbitrarily set to zero for the best fit potential. For instance, the volume integrals of the imaginary potentials vary less than ±4% from the average value. Significant differences are encountered in the imaginary diffuseness values, which are $a=0.513$, 0.537, and 0.767 fm for the unfolded, phenomenological, and folded potentials, respectively. These differences are reflected dramatically in the calculations shown in Fig. 11, where the smaller diffuseness values are seen to give a less rapid decrease in cross section as a function of scattering angle. It is interesting to note that, on the basis of this single case, the unfolded or Johnson-Soper type of potential appears to give a much better description of intermediate energy elastic deuteron scattering than does the folded or Watanabe type. This is the opposite of what is expected theoretically and observed experimentally at lower energies (see, e.g., Refs. 73, 75, and 76).

E. Extension to multiple step processes—the CCBA

The reaction theory embodied in the DWBA assumes that the pickup process occurs in a single direct step. However, it has been known for some time[13,31,84] that multiple step processes can be important in the (p,d) reaction, especially when the direct process is suppressed for some reason. The increased importance of multistep processes in the ^{12}C(p,d) reaction as the proton energy is increased into the intermediate energy region has been discussed extensively by Källne and Obst.[13] Considerable experimental evidence that this is a general property of the intermediate energy reaction was presented in Sec. III.

Multistep processes have been treated theoretically at lower energies using coupled-channels extensions of the DWBA, either the coupled-reaction channels (CRC) (Ref. 85) or coupled-channels-Born-approximation (CCBA) (Ref. 86) formalisms. The multistep calculations to be presented below were performed using the program CHUCK (Ref. 87) which incorporates the standard form of the (CRC) which will not be discussed in detail here.

F. Numerical considerations and input sensitivities

The exact-finite range (EFR) and zero-range (ZR) distorted wave Born approximation calculations to be presented below were performed using the codes DWUCK5 and DWUCK4,[87] respectively. Zero range (ZR) coupled channels Born approximation (CCBA) calculations were done with the program CHUCK.[87] In all calculations, 50 partial waves were used to describe the proton and deuteron channels. Test calculations employing up to 70 partial waves indicated that 50 were adequate. Parameters for the radial integrations were the following: step size or $DR=0.025$–0.030 fm and upper radial limit or $RMAX=10$–12 fm, the smaller values being used for the

lighter targets, the larger values for the heavier ones. Again, test calculations showed that results were stable against changes in these parameters.

The importance of an EFR treatment of the deuteron D state in the (p,d) reaction at intermediate energies has been discussed often.[1,10,11] It has also been known[1,10] that ZR calculations can qualitatively reproduce the EFR results, apart from an overall normalization factor. In Fig. 12 EFR and ZR results are compared for the $^{13}C(p,d)^{12}C(4.44\ MeV\ 2^+)$ transition. The ZR result has arbitrarily been normalized to the EFR calculation (which includes the D state) and this normalization corresponds to an effective $D_0 = -80\ MeV^{3/2}$ compared to the low energy value of $-125\ MeV\ fm^{3/2}$. Qualitative agreement is indeed observed, although noticeably more structure is apparent in the ZR results.

In Secs. IV A and IV B it was noted that the (p,d) cross section as given by the PWBA depends simply and directly on a physically interesting quantity, the Fourier transform of the bound-neutron wave function. It is important to establish to what extent this dependence is modified by the presence of distortions. Figure 10, discussed in Sec. IV C, displays momentum space $n + {}^{11}C$ $1p_{3/2}$ wave functions generated using Woods-Saxon wells with geometries taken from Refs. 65 and 68. A harmonic oscillator wave function having the same $\langle r^2 \rangle$ value is also displayed. Appreciable differences in these momentum space wave functions can be observed and these are directly reflected in the ZR PWBA cross sections appearing in Fig. 13. The corresponding ZR DWBA calculations appear below in Fig. 13. The harmonic oscillator result—which was perfectly smooth in the PWBA—now has structure in its angular distribution which is similar to that observed for the Woods-Saxon bound states. As demonstrated in Fig. 14, exact finite range and deuteron

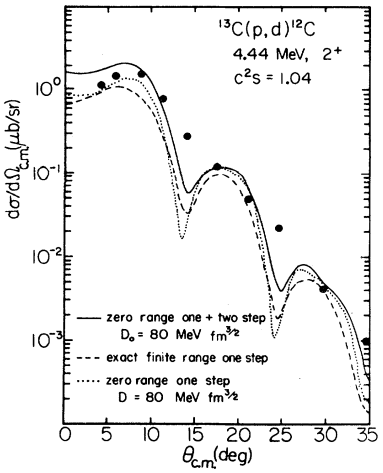

FIG. 12. Calculations for the 800 MeV $^{13}C(p,d)^{12}C(4.44\ MeV\ 2^+)$ reaction. The dashed line is a one-step EFR result normalized with a spectroscopic factor of $C^2S = 1.038$. The ZR coupled-channels calculations using the coupling scheme shown and single-step calculations are represented by solid and dotted lines, respectively, and both are normalized using $D_0 = -80$ MeV fm$^{3/2}$. Transfer amplitudes were calculated from the wave functions of Ref. 23.

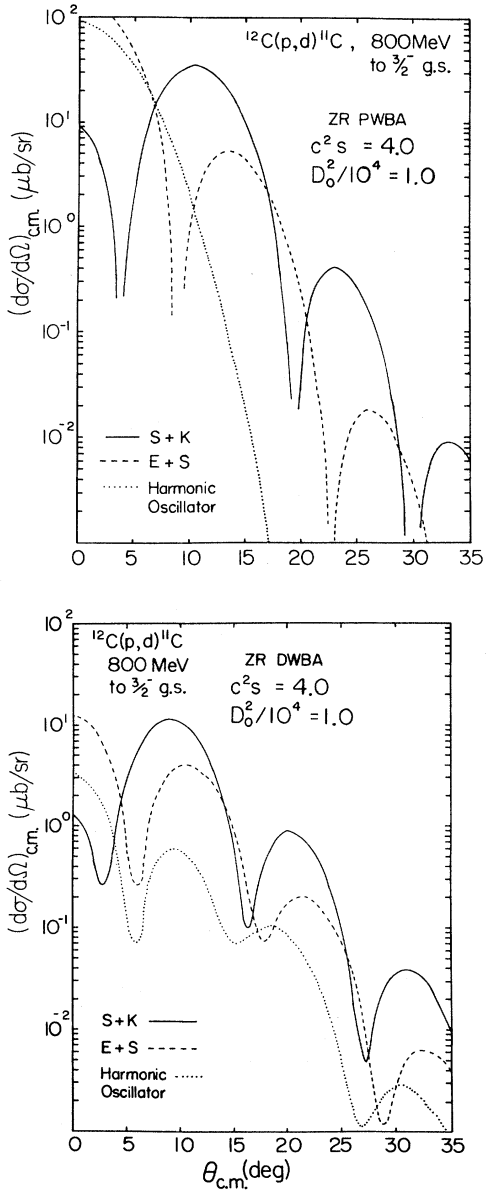

FIG. 13. Plane wave calculations to illustrate the sensitivity of (p,d) cross sections to the neutron bound state are shown above, with curves corresponding to those of Fig. 10. Below are shown the predictions using the same bound states in the DWBA, using the zero range approximation, with $C^2S = 4.0$, $D_0 = -100\ MeV\ fm^{3/2}$.

D-state effects, treated with the EFR DWBA, tend only to wash out somewhat the structure observed in the ZR calculations. Taken together, these calculations show that, while some sensitivity to details of the nuclear bound state is present in the EFR DWBA calculations, the distortions play a very important, possibly dominant, role in determining the structure which is present in the (p,d) angular distribution. The simple dependence on the bound state wave function suggested by the PWBA is not observed and it must be concluded that the extraction of information about the high momentum components of this

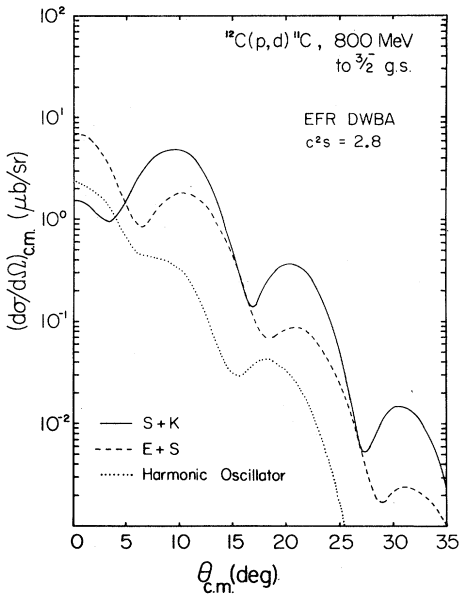

FIG. 14. Exact finite range predictions are shown for the same neutron bound states assumed in Fig. 13, using $C^2S=2.8$ (Ref. 23).

wave function from intermediate energy (p,d) data will be very difficult, at best.

The sensitivity of the calculations to ambiguities in the proton and deuteron optical model potentials was investigated on a limited basis. Zero range calculations for the ^{40}Ca(p,d)^{39}Ca($\frac{3}{2}^+$,g.s.) transition were done using the p + ^{12}C and p + ^{58}Ni phenomenological potentials of Table IV with radii appropriately scaled by $A^{1/3}$. These results show that, while the slight oscillatory structure present in the calculations is affected by the variation of these parameters, the general features of the calculated angular distribution, such as overall magnitude and slope, are unchanged.

Sensitivity to deuteron optical potentials was found to be greater than that for protons. Test calculations showed that 40% variations in the geometry of the deuteron imaginary potential could produce significant changes in the calculated (p,d) cross sections, including shifts in overall normalization of a factor of 3. Comparisons between EFR calculations employing the folded (Watanabe) and unfolded (Johnson and Soper) deuteron potentials will be made below for the ground state transitions of several nuclei. The conclusions drawn from those comparisons can be summarized by saying that use of the folded potential, with its large diffuseness value and larger rms radius, results in (p,d) cross sections which are smaller by factors of 2 or 3 and more highly structured than those obtained with the unfolded potential.

Some effort was made to gauge the importance of the nuclear interior in these reactions. In general, reactions with good momentum matching (i.e., $j_{\text{transfer}} = |\vec{k}_{\text{in}} - \vec{k}_{\text{out}}| R$, where j_{transfer} is the angular momentum transfer, k is the wave number in the incident or outgoing channel, and R is the nuclear radius) are known to be surface dominated.[63] As the momentum match worsens for the (p,d) reaction as the bombarding energy increases, more and more of the nuclear volume contributes and, typically, the sensitivity of DWBA calculations to input parameters—especially the distorting potentials—increases.[31,78] On the other hand, the optical potentials at these energies are extremely absorptive. In a semiclassical picture (and ignoring the effects of reflections and refraction), an 800 MeV proton suffering a head-on collision with an ^{16}O nucleus has only a 5% probability of passing through that nucleus while a deuteron has only a 1% probability. This absorptivity obviously serves to reduce the contribution from the interior of the nucleus.

To examine the role of the nuclear interior in the reactions studied here, ZR DWBA calculations were performed with various lower cutoffs in the radial integrations. Test calculations show that for the ^{12}C(p,d)^{11}C($\frac{3}{2}^-$,g.s.) transition, the innermost 1 fm contributes substantially. For the ^{40}Ca(p,d)^{39}Ca($\frac{3}{2}^+$,g.s.) transition, a 1 fm lower cutoff has a negligible effect while at 2 fm substantial changes begin to appear. Keeping in mind that the radii of ^{12}C and ^{40}Ca are approximately 2.3 and 3.4 fm, respectively, these results suggest that roughly the outer 2 or 2.5 fm of the nuclear volume are active in the (p,d) reaction at $T_p=800$ MeV. The calculations also show that the interior contributions interfere destructively with the surface contributions and that the degree of cancellation is extreme.

G. Comparison of DWBA calculations with data

EFR DWBA calculations have been compared with intermediate energy ^{4}He,[11,12] ^{7}Li,[9] ^{12}C,[10] and ^{13}C (Ref. 9) (p,d) data on a limited basis in several previous publications. Those calculations are similar to those to be discussed below except that more care has been exercised in the present work in generating a consistent set of input parameters, especially for the distoring potentials. The material to be presented below is also of a much greater scope and represents the first systematic application of the EFR DWBA to a large body of 800 MeV (p,d) data. Theoretical nuclear spectroscopic factors are used to make possible a consistent comparison between the magnitudes of the data and the predictions, and only the states of best known structure are used as examples.

1. ^{7}Li(p,d)^{6}Li

EFR DWBA calculations are compared with experimental cross sections for the 1^+ ground state and the 2.18 MeV 3^+ levels in Fig. 5. The spectroscopic factors used to normalize the calculations were calculated using a simple rotational model of ^{7}Li, assuming the ground state to be a member of the [110] $K=\frac{1}{2}$ band. A deformation parameter of $\beta=+0.77$ was assumed[88] and the spherical expansion coefficients of the intrinsic state were determined by numerically solving the coupled-channels bound-state problem using a deformed Woods-Saxon well and requiring that the resulting wave functions give the observed charge rms radius and electric quadrupole moment. As can be seen in Fig. 5, calculations using folded and unfolded deuteron potentials give similar results. For the 1^+

ground state the calculations lie slightly below the data and relative minima predicted at $\theta=17°$ and 32° do not appear in the measurements. The overall rate of decrease as a function of angle is correctly predicted. The calculations underestimate the cross section for the 2.185 MeV 3^+, $T=0$ level by at least a factor of 6. This is a direct result of the enhancement at intermediate energies of the 3^+ level relative to the ground state which was discussed at length in Sec. III B. The physics responsible for this enhancement is evidently not contained in the EFR DWBA used here. Zero-range coupled-channels calculations using rotational-model spectroscopic amplitudes show that conventional multistep effects are quite small for both the 1^+ and 3^+ transitions and do not account for the observed enhancement, the origin of which remains unknown.

2. $^{12}C(p,d)^{11}C$

EFR DWBA calculations using folded and unfolded deuteron potentials are compared with the cross sections for the $\frac{3}{2}^-$ ground state of ^{11}C in Fig. 15. The calculations are normalized using a spectroscopic factor of $C^2S=2.8$ calculated from the wave functions of Norton and Goldhammer.[23] Both calculations reproduce well the general rate of falloff as a function of scattering angle. However, the calculation using the folded potential, while having the correct magnitude, overpredicts the amount of structure in the angular distribution. Use of the unfolded potential results in an overprediction of the cross section by about a factor of 2 but gives a good reproduction of the shape. The calculations are similar to those presented in Ref. 10 for the same reaction at $T_p=700$ MeV where optical potentials and calculational procedures were slightly different.

The $^{12}C(p,d)^{11}C$ reaction at the present energies strongly excites levels such as the first $\frac{5}{2}^-$ and $\frac{7}{2}^-$ states whose excitation is forbidden in the single-step pickup model. Källne and Obst[13] and others[31] have suggested that these state are populated via multistep processes involving inelastic transitions in both the proton and deuteron channels. In the present work, this speculation has been tested by performing zero-range CCBA calculations for the $\frac{3}{2}^-$ ground state and 6.48 MeV $\frac{7}{2}^-$ levels. The important couplings considered are those arising from the level parentages indicated schematically in Fig. 16. The inelastic amplitudes were determined from experiment[31,89] and the transfer amplitudes from the wave functions of Norton and Goldhammer.[23] Calculations using these amplitudes reproduce $^{12}C(p,d)^{11}C$ data at $T_p=121$ MeV quite well.[31] Our calculations are compared with the 800 MeV data in Fig. 15. The overall zero-range normalization was fixed by requiring that the $\frac{3}{2}^-$ calculation agree in magnitude with the data. The calculated $\frac{7}{2}^-$ cross section, thus normalized, is seen to agree quite well with experiment. These findings are consistent with those of Baker *et al.*[1] and Källne and Obst[13] and suggest that conventional multistep processes provide a reasonable explanation of the presence of strong forbidden levels in the $^{12}C(p,d)^{11}C$ spectrum and further indicate the importance of such mechanisms in the intermediate energy (p,d) reaction.

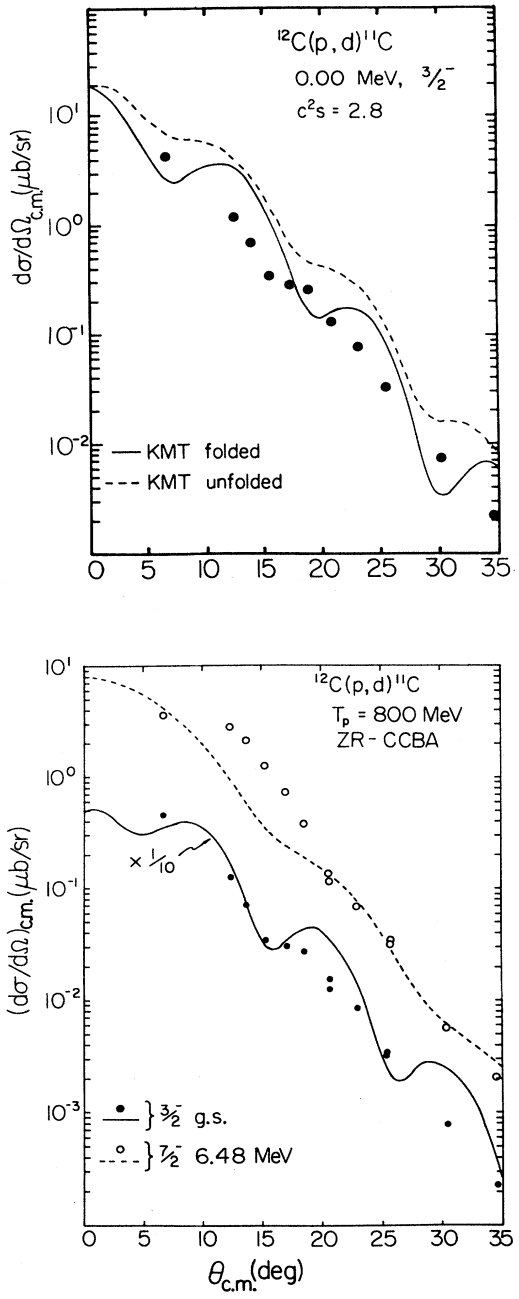

FIG. 15. Above are shown EFR calculations for the ground state of ^{11}C using folded or unfolded deuteron potentials, as described in the text. Below are shown CCBA predictions for the $\frac{3}{2}^-$ and $\frac{7}{2}^-$ states.

The possibility that multiple step processes are responsible for the previously unobserved 2 MeV broad region of excitation centered at 13.2 MeV in ^{11}C (see Fig. 2) was investigated using the ZR CCBA. Blanpied *et al.*[35,36] and Ray *et al.*[37] have observed that the two-step excitation of the 14.1 MeV 4^+ level of ^{12}C in 800 MeV proton inelastic scattering is quite strong with cross sections comparable to those for the 4.44 MeV 2^+ state at the larger angles.

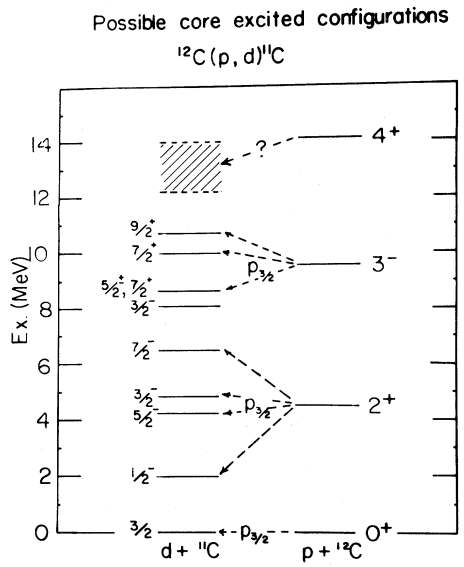

FIG. 16. Possible correlations between the states of ^{12}C and the high spin states excited in the present work in ^{11}C are indicated.

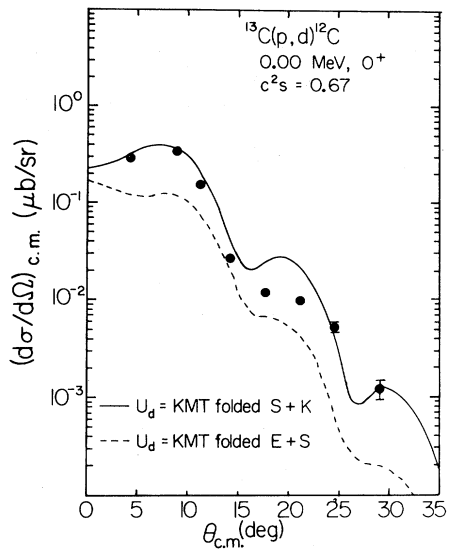

FIG. 17. Data to the ground state of ^{12}C are compared to EFR calculations as described in the text, using bound states computed with the geometry of Ref. 68 (*S* and *K*) or Ref. 65 (*E* and *S*).

The plausible assumption can then be made that the level or levels at 13.2 MeV are excited by the inelastic excitation of the 4^+ state in ^{12}C followed by the pickup of a $1p$ neutron leading to levels with $\frac{5}{2}^- < J < \frac{11}{2}^-$. High-spin negative-parity levels with appreciable parentage based on the 4^+ level are predicted in this region by Norton and Goldhammer,[23] for example. To test this notion we performed ZR CCBA calculations using the inelastic amplitudes of Ray *et al.*[37] and simple weak coupling transfer amplitudes. These calculations drastically underestimate (by a factor of 50) the observed cross sections and it must be concluded the preceding interpretation of the 13.2 MeV level is inadequate.

Another plausible interpretation is that the 13.2 MeV level arises from $1s_{1/2}$ neutron pickup and, indeed, EFR DWBA calculations with $C^2S=2.0$ are in rough agreement with the data. However, similar calculations predict a very large cross section at $T_p=121$ MeV when in fact none is observed[56] at this or other energies[10,20] below 200 MeV. Furthermore, other experiments[90] have shown the bulk of the $1s_{1/2}$ pickup strength to lie much higher in excitation energy, near 19.5 MeV, and to have a width of nearly 10 MeV. Consequently this explanation of the 13.2 MeV level or levels must also be ruled out.

While the mechanism of excitation is unknown, it seems quite probable that the 13.2 MeV region of excitation corresponds to a cluster of unresolved high spin states. In addition to the levels predicted theoretically by Norton and Goldhammer[23] and discussed above, high spin assignments have been made experimentally in the mirror nucleus, ^{11}B, at excitation energies of 13.12 ($\frac{9}{2}^-$), 13.16 ($\frac{5}{2}^+, \frac{7}{2}^+$), and 14.02 MeV ($\frac{11}{2}^+$).[91]

3. $^{13}C(p,d)^{12}C$

EFR DWBA calculations using a folded deuteron potential are compared with data for the 0^+ g.s. transition in Fig. 17. The overall normalization is fixed—as for all calculations of the $^{13}C(p,d)^{12}C$ reaction presented in this section—by spectroscopic factors calculated from the wave functions of Norton and Goldhammer.[23] The calculations using the bound state wave functions of Shepard and Kaczkowski[68] reproduce the data quite well in both shape and magnitude. In particular, the relative maximum near 7.5° is correctly described and the oscillatory structure at larger angles is qualitatively reproduced. Use of the Elton and Swift wave function[65] results in somewhat poorer agreement with the data.

Similar calculations using the bound state wave functions of Shepard and Kaczkowski[68] are compared with the data for the 12.7 MeV 1^+ $T=0$, the 15.1 MeV 1^+ $T=1$, and 16.1 MeV 2^+ $T=1$ levels in Fig. 18. Again, the agreement in shape and magnitude is quite good, although at a detailed level is appears that the Q-value dependence in these $1p$ pickup processes is overestimated by the DWBA. That is, the DWBA overestimates the difference in shape between the ground state angular distribution of Fig. 17 and those for the excited states in Fig. 18.

Several types of calculations were performed for the transition to the 4.44 MeV 2^+ level and they are compared with the data in Fig. 12. The dashed curve represents an EFR DWBA calculation which is in reasonably good agreement with the data, although having appreciably more structure. Also shown are ZR CCBA calculations, the dotted curve including the direct, one-step contribution only, normalized to the EFR calculation and the other, solid curve, utilizing the same transfer normalization, but including all the couplings indicated in Fig. 19. These latter CCBA results suggest that, while two-step effects are not large for this transition, they do serve to increase the cross section slightly and wash out the structure. Both of these effects would improve the agreement between the EFR calculations, which because of calculational limitations include only the direct process, and

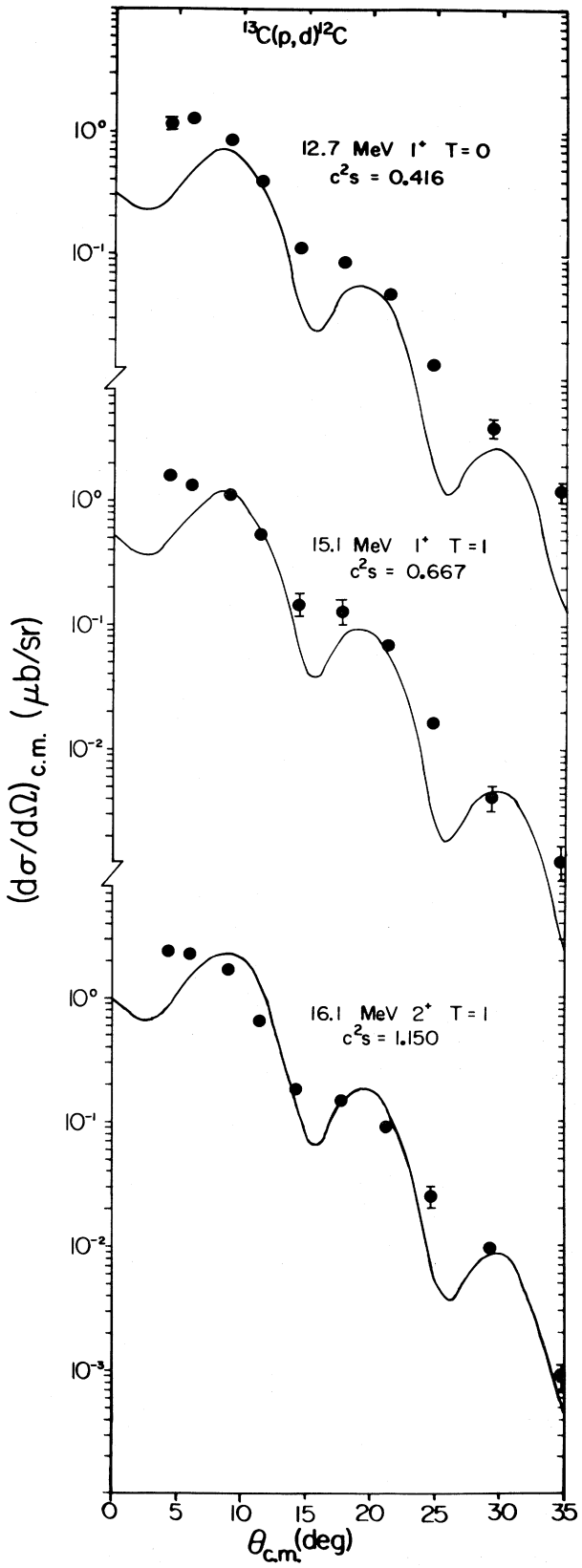

FIG. 18. Data for pickup for three high-lying simple states of ^{12}C are compared to EFR DWBA predictions, as in the solid curve of Fig. 17.

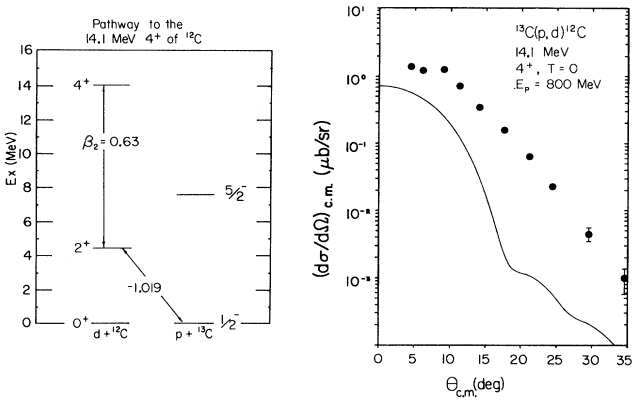

FIG. 19. Data to the 14.1 MeV 4^+ state of ^{12}C are compared to a ZR CCBA prediction using the coupling scheme indicated, using $D_0 = -80$ MeV fm$^{3/2}$.

the data. In this regard, it should be noted that the ground state angular distribution, where two-step contributions are quite small, has much sharper structure experimentally than the 4.44 MeV 2^+ level.

Two-step calculations were also performed for the transition to the 14.1 MeV 4^+ $T=0$ level employing the coupling scheme shown in Fig. 19. In this case, there is no direct amplitude and the transition must occur in at least two steps. The ZR CCBA calculation is compared with the data in Fig. 19 and, while the shape is qualitatively reproduced, the magnitude of the cross section is underpredicted by a factor of 2 or 3. This may be due to the limited number of couplings which were included in the calculations due to computational limitations. Specifically, the strong inelastic couplings in the $p + ^{13}C$ channels which were omitted might reasonably be expected to increase substantially the computed cross sections. In fact, estimates based on a rotational model of ^{13}C suggest that the coupling through the 7.55 MeV $\frac{5}{2}^-$ level of ^{13}C would increase the 4^+ cross section by a factor of 2.25, roughly what is required for agreement with experiment at the forward angles. In any case, the agreement is good enough to suggest that the two-step processes indicated in Fig. 19 provide a plausible explanation for the excitation of the 4^+ level.

4. $^{16}O(p,d)^{15}O$

EFR DWBA calculations are compared with data for the transition to the $\frac{1}{2}^-$ ground state in Fig. 20. Normalization is obtained by assuming the full sum rule spectroscopic factor, $C^2S = 2.0$. As usual, calculations were performed using both folded and unfolded theoretical deuteron potentials. As discussed above in Sec. IV D, ^{16}O is a unique case since, for this target only, reliable deuteron elastic scattering data exist at a relevant energy [$T_d = 700$ MeV (Ref. 4)] and it is therefore possible to do the DWBA calculations using a phenomenological potential. The results of such a calculation also resemble closely those obtained with the unfolded theoretical potential. This is not surprising considering the similarity of the potentials (see Table IV) and their elastic scattering predictions (see Fig. 11). These calculations overpredict the

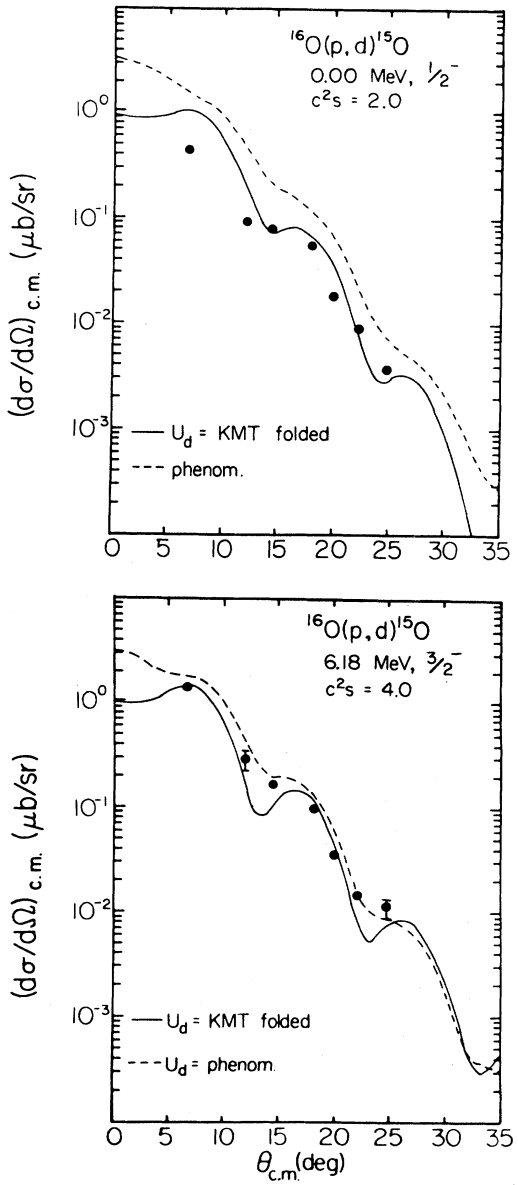

FIG. 20. Data for the strong simple hole states of ^{15}O are compared to EFR predictions using KMT and best fit optical model parameters for the deuteron.

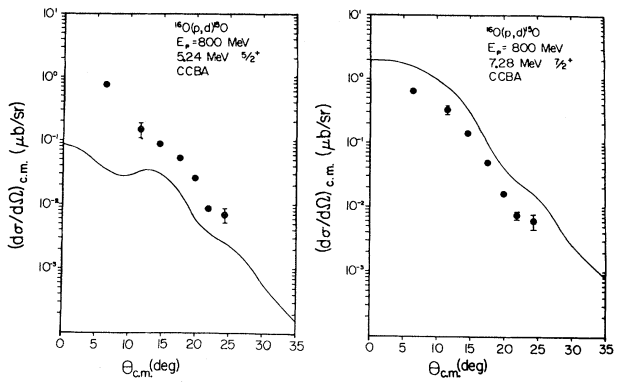

FIG. 21. Pickup data to $\frac{5}{2}^+$ and $\frac{7}{2}^+$ states in ^{15}O are compared to zero range CCBA calculations, proceeding through the strong 3^- state of the ^{16}O target, with $D_0 = -80$ MeV fm$^{3/2}$.

magnitude of the data by about a factor of 2 to 3. The calculation using the folded deuteron potential reproduces the experimental shape and magnitude reasonably well. Similar calculations are compared with data for the transition to the 6.18 MeV $\frac{3}{2}^-$ level in Fig. 20 where similar agreement is again observed with a normalization assuming the full sum rule spectroscopic factor of 4.

It is interesting to note that similar calculations done for the ^{16}O(d,p)^{17}O($\frac{5}{2}^+$,g.s. and 0.87 MeV $\frac{1}{2}^+$ state) reaction at $T_d = 700$ MeV (Ref. 95) reproduce the data[4,8] perfectly when the phenomenological deuteron potentials are used but are too low by a factor of 2 with the folded potential. It is not understood why this difference between the (p,d) and (d,p) reactions on ^{16}O exists although it may be traceable to the very different binding energies of the transferred neutrons [15 MeV for (p,d) and 3 MeV for (d,p)] and the resulting differences in their wave functions. It should be pointed out that the neutron well geometry used was the same for both the (p,d) and (d,p) calculations and that, since it was determined by requiring consistency with $e^- + ^{16}$O elastic scattering data (see Sec. IV C), it is, strictly speaking, only appropriate for the (p,d) calculations.

Two-step ZR CCBA calculations were performed for the 5.2 MeV $\frac{5}{2}^+$ and 7.2 MeV $\frac{7}{2}^+$ levels. In both cases, a single intermediate state, the highly collective 6.13 3^- level of ^{16}O, was included. The transfer amplitudes were computed using a simple weak coupling model; i.e., $(3^- \times p_{1/2}^{-1})_{J^\pi = 5/2^+, 3/2^+}$. Normalization of the zero-range calculations was established by requiring that the ground state cross sections be reproduced. These calculations are compared with the data in Fig. 21 where it can be seen that the $\frac{7}{2}^+$ angular distribution is qualitatively reproduced, but that for the $\frac{5}{2}^+$ is poorly described, both in shape and magnitude. It is possible that the reason for the discrepancy between the $\frac{5}{2}^+$ and $\frac{7}{2}^+$ agreement lies in the artificial limitation on angular momentum transfers imposed by the zero-range (S state only) approximation in the transfer step and that EFR CCBA calculations would be in better correspondence with experiment. Again, the level of agreement is sufficient to support the hypothesis that conventional multistep processes are mainly responsible for the excitation of these levels.

5. ^{26}Mg, ^{28}Si, and ^{40}Ca(p,d)

EFR DWBA calculations are compared with data for the ground state transitions of the ^{25}Mg, ^{28}Si, and ^{40}Ca(p,d) reactions in Fig. 22. The spectroscopic factors used to normalize the ^{25}Mg (Ref. 43) and ^{28}Si (Ref. 93) calculations were computed using the rotational model. The spectroscopic factor for ^{40}Ca was obtained from analyses by Kunz.[94] For ^{25}Mg and ^{28}Si, the calculations using the folded potentials agree quite well in magnitude with the data, although they overpredict the amount of structure in the angular distributions. Use of the unfolded potentials results in overprediction of the data by about a

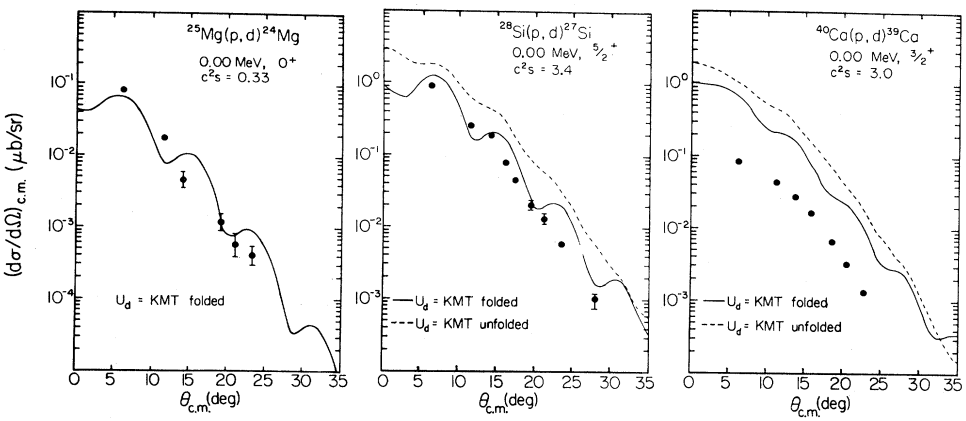

FIG. 22. Pickup data for ground state transitions for the three heavier targets of the present study are compared to the EFR DWBA prediction using two KMT optical potentials.

factor of 2 for these targets.

The situation for ^{40}Ca is markedly different. As noted in Sec. III I, the experimental cross section for the ^{40}Ca(p,d)^{39}Ca($\frac{3}{2}^+$,g.s.) transition is roughly an order of magnitude smaller than typical cross sections for the lighter targets. Figure 22 shows that this drop in cross section is not reproduced by the ER DWBA calculations which overestimate the data by factors of 5 to 10. The origin of this discrepancy is unknown.

V. SUMMARY AND CONCLUSIONS

Experimentally there are striking similarities and differences between low energy (p,d) data and the 800 MeV measurements presented in Sec. III. The strong single-hole states observed at lower energies are populated in the present work. Generally speaking, the relative intensities of these levels are different at the present energies, but these differences can be anticipated based on an extrapolation of the energy dependence at lower energies. Furthermore, they can be understood physically as arising from the increasingly severe momentum mismatch at the higher energies, favoring the excitation of high spin levels.

It is also true that there are some important differences which could not be anticipated and which as yet are not understood. In all cases except lithium, very strong levels at high excitation are observed which have no precedent in lower energy (p,d) measurements. In several instances—^{12}C, ^{16}O, ^{28}Si, and ^{40}Ca—broad regions of strength are observed between 10 and 20 MeV of excitation in the residual nucleus. There is no indication that deep single-hole states are preferentially excited in the (p,d) reaction at these energies.

The angular distributions extracted for the strong transitions in the present measurements differ from their low energy counterparts in that there is no clear signature of the angular momentum transfer in their shapes. In all cases, angular distributions show a relatively featureless, nearly monotonic decrease as a function of angle.

Theoretically, we have chosen to apply a low-energy model of the reaction—the DWBA—to the present intermediate energy data. In so doing several considerations unique to the intermediate energy regime need to be addressed. First, a consistent treatment requires that the structure of the deuteron be treated explicitly using exact-finite-range (EFR) techniques. Use of the zero-range (ZR) approximation results in an unnormalized theory, although many of the features of the EFR calculations persist. Also, since the PWBA (p,d) amplitude is sensitive to high Fourier components in the bound neutron wave function—indeed determination of these components was one of the original motivations for doing intermediate energy (p,d) measurements—care was taken to ensure that the wave functions used have high momentum components consistent with elastic electron scattering data. Calculations reveal, however, that the presence of distortions in the proton and deuteron channels reduces the sensitivity of the (p,d) amplitude to details of the nuclear bound state and that shapes of calculated angular distributions may be dominated by distortion effects. This point is discussed in some detail in a paper by Shepard and Rost.[95]

It is then evident that care must be taken to describe distortion effects as accurately as possible. Determination of optical potentials for the proton channel is relatively straightforward because of the wealth of relevant data and the extensive theoretical interest in intermediate energy proton scattering. The situation is quite different for the deuteron potentials, however, due both to a scarcity of data and to theoretical ambiguities. This is all the more unfortunate since the calculations are more sensitive to the deuteron distortions. In the present work, two types of theoretical deuteron potentials based on the KMT multiple scattering theory[70,71] and simple folding ideas[73,74] were used. These potentials were found to be quite similar to one another and reassuringly similar to a phenomenological potential determined by fitting the one set of reliable intermediate energy deuteron elastic scattering data, namely the 698 MeV d + ^{16}O results from Saclay.[4]

Calculations also show that, in spite of the very absorptive nature of the proton and deuteron optical potentials, a large fraction of the nuclear volume contributes to the re-

action amplitude. The (p,d) reaction at these energies is not a surface dominated process. Furthermore, the degree of cancellation between surface and interior contributions is evidently very strong, indicating that any theoretical treatment of the problem must treat the entire volume of the nucleus carefully.

The DWBA calculations—with no free parameters—are seen to be in good qualitative agreement with many of the strong transitions which are known from low energy studies to lead to predominantly single hole states. The general rate of falloff as a function of angle is invariably well reproduced. In many cases the calculations also describe qualitatively the structure observed in the measured angular distributions although the predicted structure is sensitive to the choice of deuteron optical potentials. Relative strengths of levels are also generally well reproduced. Absolute magnitudes of the calculations are sensitive to the choice of deuteron optical potentials. When folded KMT potentials are used, magnitudes are quite well reproduced, while use of the unfolded potential [and, for ^{16}O(p,d), the phenomenological potential] gives cross sections which are factors of 2 to 3 larger than the data.

For the ^{12}C, ^{13}C, and ^{16}O(p,d) reactions, transitions strongly suspected of being excited through multistep processes[13] are reasonably well described by zero-range, coupled-channels calculations. Calculational restrictions prohibit treatment of EFR effects or the use of complete coupling schemes and thus limit the conclusions which can be drawn. Nevertheless, the level of agreement is sufficently good to suggest that conventional multistep processes, familiar from lower energy analyses, are largely responsible for the excitation of these levels.

This work was supported in part by the U.S. Department of Energy.

*Present address: TRIUMF, 4004 Wesbrook Mall, Vancouver, British Columbia, Canada.
†Present address: MP-10, LAMPF, Los Alamos National Laboratory, Los Alamos, NM 87545.
‡Present address: Department of Physics, University of South Carolina, Columbia, SC 29208.
§Present address: Faculty of Science, University of Jordan, Amman, Jordan.
**Present address: University of Texas, Austin, TX 78712.

[1]S. D. Baker *et al.*, Phys. Lett. **52B**, 57 (1974).
[2]T. Bauer *et al.*, Phys. Lett. **67B**, 265 (1977).
[3]J. Berger *et al.*, Lett. Nuovo Cimento **19**, 287 (1977).
[4]G. Bruge, Saclay Internal Report DPh-N/ME/78-1, 1978.
[5]J. Källne *et al.*, Phys. Rev. Lett. **41**, 1638 (1978).
[6]J. Källne *et al.*, Phys. Rev. C **21**, 675 (1980).
[7]R. Liljestrand *et al.*, Phys. Lett. **99B**, 311 (1981).
[8]A. Boudard *et al.*, Phys. Rev. Lett. **46**, 218 (1981).
[9]T. S. Bauer *et al.*, Phys. Rev. C **21**, 757 (1980).
[10]E. Rost and J. R. Shepard, Phys. Lett. **59B**, 413 (1975).
[11]E. Rost, J. R. Shepard, and D. A. Sparrow, Phys. Rev. C **17**, 1513 (1978).
[12]J. R. Shepard, E. Rost, and G. R. Smith, Phys. Lett. **89B**, 13 (1979).
[13]J. Källne and A. W. Obst, Phys. Rev. C **15**, 477 (1977).
[14]H. Howard, LAMPF Users Handbook, Los Alamos Scientific Laboratory Report MP-DO-1-UMB, 1974.
[15]B. E. Bonner *et al.*, Phys. Rev. C **17**, 671 (1978).
[16]D. E. Prull (unpublished).
[17]D. W. Devins *et al.*, Nucl. Phys. **A126**, 261 (1969).
[18]L. A. Kull, Phys. Rev. **163**, 1066 (1967).
[19]J. K. P. Lee, S. K. Mark, P. M. Portner, and R. B. Moore, Nucl. Phys. **A106**, 357 (1968).
[20]D. Bachelier *et al.*, Nucl. Phys. **A126**, 60 (1969).
[21]J. Källne, B. Fagerström, O. Sundberg, and G. Tibell, Phys. Lett. **52B**, 313 (1974).
[22]R. Liljestrand *et al.* (private communication); and (unpublished).
[23]J. L. Norton, Ph.D. thesis, University of Kansas, 1970; J. L. Norton and P. Goldhammer, Nucl. Phys. **A165**, 3 (1971).
[24]C. Glashausser and M. E. Rickey, Phys. Rev. **154**, 1033 (1967).
[25]N. S. Chant, P. S. Fischer, and D. K. Scott, Nucl. Phys. **A99**, 669 (1967).
[26]F. E. Bertrand *et al.*, Nucl. Instrum. Methods **101**, 475 (1972).
[27]L. J. Parish *et al.*, Phys. Rev. C **9**, 876 (1974).
[28]B. Fagerström and J. Källne, Phys. Scr. **8**, 14 (1973).
[29]P. G. Roos *et al.*, Nucl. Phys. **A255**, 187 (1975).
[30]A. Ingemarsson and G. Tibell, Phys. Scr. **10**, 159 (1974).
[31]J. R. Shepard *et al.*, University of Colorado Nuclear Physics Laboratory Technical Progress Report NPL-793, 1977, p. 123; and (unpublished).
[32]P. D. Kunz and E. Rost, Phys. Lett. **53B**, 9 (1974).
[33]R. N. Singh *et al.*, Nucl. Phys. **A205**, 97 (1973).
[34]F. Ajzenberg-Selove, Nucl. Phys. **A336**, 1 (1980).
[35]G. S. Blanpied *et al.*, Phys. Rev. Lett. **39**, 1447 (1977).
[36]G. S. Blanpied *et al.*, Phys. Rev. C **18**, 1436 (1978).
[37]L. Ray *et al.*, Phys. Rev. Lett. **40**, 1547 (1978).
[38]D. K. Scott *et al.*, Nucl. Phys. **A141**, 497 (1970).
[39]H. Taketani, J. Muto, H. Yamaguchi, and J. Kokame, Phys. Lett. **27B**, 625 (1968).
[40]S. K. Datta, G. P. A. Berg, and P. A. Quin, Nucl. Phys. **A312**, 1 (1978).
[41]J. D. Cossairt and D. P. May, Nucl. Phys. **A319**, 182 (1979).
[42]J. Snelgrove and E. Kashy, Phys. Rev. **187**, 1246 (1969).
[43]G. Delic, Nucl. Phys. **A158**, 117 (1970).
[44]C. D. Kavaloski, G. Bassani, and N. M. Hintz, Phys. Rev. **132**, 813 (1963).
[45]F. El-Bedevi, M. Shalab, A. Khazbak, and F. Raoof, J. Phys. G **1**, 749 (1975).
[46]E. F. Bennett, Phys. Rev. **122**, 595 (1961).
[47]R. E. Tribble, G. T. Garvey, and J. R. Comfort, Phys. Lett. **44B**, 366 (1973).
[48]G. D. Jones, R. R. Johnson, and R. J. Griffiths, Nucl. Phys. **A107**, 659 (1968).
[49]R. L. Kozub, Phys. Rev. **172**, 1078 (1968).
[50]H. Ohnuma *et al.*, J. Phys. Soc. Jpn. **42**, 382 (1977).
[51]D. A. Miller, D. W. Devins, and W. P. Jones, Indiana University Cyclotron Facility Scientific and Technical Reports, 1979, p. 92; and (unpublished).
[52]E. Gerlic *et al.*, Phys. Rev. C **12**, 2106 (1975).
[53]J. van de Wiele, E. Gerlic, H. Langevin-Joliot, and G. Dunhamel, Nucl. Phys. **A297**, 61 (1978).
[54]C. A. Whitten, Jr., M. C. Mermaz, and D. A. Bromley, Phys. Rev. C **1**, 1455 (1970).
[55]P. M. Endt and C. van der Leun, Nucl. Phys. **A310**, 1 (1978).
[56]D. A. Miller (private communication); and (unpublished).

[57]P. Doll, G. J. Wagner, K. T. Knopfle, and G. Mairle, Nucl. Phys. **A263**, 210 (1976).
[58]N. S. Chant and J. M. Nelson, Nucl. Phys. **A117**, 385 (1968).
[59]H. Ejiri *et al.*, J. Phys. Soc. Jpn. **21**, 14 (1966).
[60]G. J. Wagner, P. Doll, K. T. Knopfle, and G. Mairle, Phys. Lett. **57B**, 413 (1975).
[61]C. Glashausser, M. Kondo, M. E. Rickey, and E. Rost, Phys. Lett. **14**, 113 (1965).
[62]See, e.g., N. Austern, *Direct Nuclear Reaction Theories* (Wiley, New York, 1970), Vol. XXV, and reference contained therein.
[63]R. Stock *et al.*, Nucl. Phys. **A104**, 136 (1967).
[64]R. V. Reid, Ann. Phys. (N.Y.) **50**, 411 (1968).
[65]L. R. B. Elton and A. Swift, Nucl. Phys. **A94**, 52 (1967).
[66]B. A Brown, S. E. Massen, and P. E. Hodgson, J. Phys. G **5**, 1655 (1979).
[67]S. Gamba, G. Ricco, and G. Rottigni, Nucl. Phys. **A213**, 383 (1973); M. Cooper and H. O. Meyer (private communication).
[68]J. R. Shepard and P. Kaczkowski, Bull. Am. Phys. Soc. **22**, 529 (1977); University of Colorado Nuclear Physics Laboratory Technical Progress Report NPL-793, 1977, p. 160.
[69]I. Sick and J. S. McCarthy, Nucl. Phys. **A150**, 631 (1970).
[70]A. Kerman, H. McManus, and R. M. Thaler, Ann. Phys. (N.Y.) **8**, 551 (1959).
[71]A. K. M. Feshbach, A. Gal, and J. Hüfner, Ann. Phys (N.Y.) **66**, 20 (1971).
[72]D. Zurstadt, University of Colorado, the optical model code OPTIMR (unpublished).
[73]R. C. Johnson and P. J. R. Soper, Phys. Rev. C **1**, 976 (1970).
[74]S. Watanabe, Nucl. Phys. **8**, 484 (1953).
[75]J. P. Farrell, Jr., C. M. Vincent, and N. Austern, Ann. Phys. (N.Y.) **96**, 333 (1976).
[76]N. Austern, C. M. Vincent, and J. P. Farrell, Jr., Ann. Phys. (N.Y.) **114**, 93 (1978).
[77]R. Johnson (private communication).
[78]J. R. Shepard, E. Rost, and P. D. Kunz, in *Polarization Phenomena in Nuclear Physics—1980 (Fifth International Symposium, Santa Fe)*, Proceedings of the Fifth International Symposium on Polarization Phenomena in Nuclear Physics, AIP Conf. Proc. No. 69, edited by G. G. Ohlson, R. E. Brown, N. Jarmie, M. W. McNaughton, and G. M. Hale (AIP, New York, 1981); and (unpublished).
[79]G. H. Rawitscher, Phys. Rev. C **9**, 2210 (1974).
[80]C. Bricman *et al.*, Phys. Lett. **75B**, 1 (1978).
[81]M. MacGregor, R. A. Arndt, and R. M. Wright, Phys. Rev. **169**, 1149 (1968); **173**, 1272 (1968); R. A. Arndt, R. H. Hackman, and L. D. Roper, Phys. Rev. C **9**, 555 (1974); **15**, 1002 (1977).
[82]C. W. Jaeger, H. Devries, and C. Devries, *Atomic and Nuclear Data Tables* (Academic, New York, 1974), Vol. 14, p. 479.
[83]G. Smith, Ph.D. thesis, University of Colorado, 1979; Los Alamos Scientific Laboratory Report LA-8166-T, 1980.
[84]R. J. Ascuitto, C. G. King, L. J. McVay, and B. Sorenson, Nucl. Phys. **A226**, 454 (1974).
[85]P. D. Kunz (private communication); see also S. R. Cotanch and C. M. Vincent, Phys. Rev. C **14**, 1739 (1976).
[86]S. K. Penny and G. R. Satchler, Nucl. Phys. **53**, 145 (1974).
[87]P. D. Kunz (unpublished).
[88]As determined from inelastic ^{4}He scattering data, S. A. Dickey *et al.* (unpublished).
[89]D. Newton, A. B. Clegg, G. L. Salmon, and D. J. Rowe, Nucl. Phys. **53**, 433 (1964).
[90]H. Tyren *et al.*, Nucl. Phys. **79**, 321 (1966).
[91]S. L. Hausladen, C. E. Nelson, and R. O. Lane, Nucl. Phys. **A217**, 563 (1973).
[92]J. R. Shepard and E. Rost, Phys. Rev. Lett. **46**, 1544 (1981).
[93]D. Dehnhard, Phys. Lett. **38B**, 389 (1972).
[94]P. D. Kunz (private communication).
[95]J. R. Shepard and E. Rost, Phys. Rev. C **25**, 2660 (1982).